ERROR PROBABILITY ANALYSIS FOR STBC

IN RAYLEIGH FADING CHANNELS

HU HONGJIE

NATIONAL UNIVERSITY OF SINGAPORE

2003

ERROR PROBABILITY ANALYSIS FOR STBC

IN RAYLEIGH FADING CHANNELS

HU HONGJIE

(B. Eng, Northwestern Polytechnical University, China)

A THESIS SUBMITTED

FOR THE DEGREE OF MASTER OF ENGINEERING

DEPARTMENT OF ELECTRICAL AND COMPUTER ENGINEERING

NATIONAL UNIVERSITY OF SINGAPORE

2003

Acknowledgements

I am deeply grateful to my supervisor, Professor Tjhung Tjeng Thiang, for his continuous guidance, encouragement and trust. It is his insight into the field that shows me the direction of my work. It is his confidence that makes my research work as enjoyable as possible.

I thank Dr. Dong Xiaodai, Dr. Chew Yong Huat and Dr. Chai Chin Choy for their helpful advice and support.

It's my great pleasure to work with my friends: Xu Zhemin, Zhang Rui, Xue Xiaoming, and Wei Ming. The talks with them have proved invaluable for my research work.

I would also like to thank the support from the Institute for Infocomm Research and National University of Singapore. I am deeply impressed by the efficient and harmonious working environment here.

Contents

Summary

In order to achieve higher spectrum efficiency, Multiple Input Multiple Output (MIMO) systems became a hot research topic in the later 1990s. Space-time block codes (STBC), which were proposed in [17][18], are a cost-effective way to exploit the huge potential capacity provided by MIMO systems. Simulation results in [17][22] demonstrated that the bit error rate (BER) performance of STBC is far superior to that of conventional single transmit antenna systems in flat Rayleigh fading channels. In this thesis we investigate the error rate performance of STBC, by theoretical analysis in both flat and frequency-selective Rayleigh fading channels.

For flat Rayleigh fading channels, following the approach in [33][34], closed form bit error probability expressions are derived for STBC with BPSK or QPSK modulation. Two transmit and one receive antennas are assumed in the thesis.

We extended Alamouti's decoding algorithm, which is optimum in flat fading channels, to frequency-selective fading channels. BPSK, two transmit and one receive antennas are assumed. RMS delay spread is assumed to be less than half of symbol duration. To concentrate on the effect of intersymbol interferences (ISI), we neglect the effect of AWGN and set SNR is set to infinity. A closed form average irreducible bit error rate (AIBER) expression for STBC in frequency-selective Rayleigh fading channels is derived based on the classic approach in [27][28] where a fixed symbol

sequence is firstly assumed to find ISI and AIBER, then the final AIBER is derived by averaging over all possible symbol sequences. The sequence should be long enough to include all symbols that cause interference on the symbol to be demodulated. Usually, several symbols are enough for the sequence. The probability distribution of the general quadratic form [4] is used to find the AIBER conditioned on a sequence. Our result provides an efficient way to evaluate the effects of frequency-selective fading with various forms of power delay profiles and pulse shapes on the error rate performance of STBC. This is a significant improvement over previous simulation based approach.

Numerical results show that in flat Rayleigh fading channels, STBC provided a performance comparable to that of receive diversity, which is only 3 dB better than STBC. In frequency-selective Rayleigh fading channels, our AIBER analysis result supports several conclusions. First, STBC effectively lowers the AIBER and thus it can do well even in selective fading channels. Second, the shape of power delay profile has little effect on the performance when RMS delay spread is small. Third, raised cosine pulse shape outperforms rectangular pulse shape when the roll-off factor α is larger than 0.75.

List of Figures

List of Symbols

α : roll-off factor of Raised Cosine filter

τ_{rms} : Root mean square of propagation delay spread

$a_n^{(i)}$: STBC encoded symbol for transmit antenna *i*

c_n : source information symbol

$\hat{c}_n$: symbols output from the decoder of STBC

d : normalized RMS delay spread, defined in Section 3.3

$d_m^{(i)}$: the composite impulse response of transmitter/receiver filter and multipath channel for transmit antenna i, defined in Section 3.3

$d_{m,k}$: the autocorrelation of $d_m^{(i)}$, defined in Section 5.4

$h(t,\tau)$: channel response at time *t* due to an impulse at $t-\tau$

$p_T(t)$: transmit pulse shape filter

$p_R(t)$: receiver matched filter

$p(t)$: the combined transmit and receive filter response

$R_h(\tau)$: power delay profile

x_n : source information bit

CHAPTER ONE

Introduction

1.1 Trends in Wireless Communications

With the introduction of the cellular concepts, the wireless communication industry is undergoing a revolution in both the technologies and applications. Analog voice communication is the main application of cellular communication before the 1990s. The mobile devices at that time were clumsy and expensive. Cellular users grew from 25,000 in 1984 to about 25 million in 1993 [1]. The second generation cellular communication systems, such as GSM, IS-95, adopted digital technologies and came into the market in the early 1990s. Good quality digital voice (compared with the analog one) and low speed data service, especially the Short Message Service (SMS), are their shining points. Since the digital systems have higher spectrum efficiency, smaller equipment size, better service quality, and the price became more affordable in the later 1990s, the user number exploded to about 630 million as of late 2001 [1]. Cellular communication systems are especially popular in the developing countries because firstly, cellular systems are affordable, easy to deploy and have uniform standards; secondly, the fixed public phone systems in the developing countries are

not as good as those in the developed countries. One typical example is China, which has about 200 million subscribers at the end of 2002 and its subscriber number is ranked as the first in the world.

Due to the emergence of the Internet and the increase of computing power, data applications become more and more popular. But the second generation digital systems are not designed for data applications and can only provide about 10 Kbps data rate. This speed is too slow for most data applications, such as email, web browsing and video transmission. Some technology improvements were made over the second generation systems and the name 2.5 generation (2.5G) system was coined. 2.5G systems, such as GPRS, can provide up to about 100 Kbps data rate. Many commercial GPRS systems were deployed worldwide at the end of 1990s, but the response from subscribers is mild. Some reasons are believed to have led to this problem: First of all, the charge for GPRS is still high compared with fixed access. Second, the transmission speed is still too slow for most data applications. Third, we have no “killer applications” designed for mobiles, although Multimedia Message Service (MMS) is expected to promote the usage recently.

To provide better data service, third generation (3G) cellular communication systems were initially finalized at the end of 1990s. The main standards for 3G are WCDMA [2] and CDMA2000 [3]. Both of these standards can support up to 2 Mbps data rate or more in the future. Commercial systems of WCDMA and CDMA2000 have been deployed in some places, such as Japan and Korea. However, the telecom industry is suffering from current recession and carriers are very cautious in adopting these new systems. We expect data applications and 3G systems will eventually become more mature and cheaper and more people can enjoy the fun brought about by the multimedia ability of 3G systems in the near future.

But if we compare 3G systems with fixed wire line Internet connection, the gap is still very huge: most Local Area Networks (LAN) in campus and office support 100 Mbps data rate at very low costs. For high data rate transmission, conventional cellular communication systems are uneconomical since they have to pay attention to covering wide areas, supporting highly mobile users and providing seamless handover. Wireless LAN was proposed to address the problem. Compared with cellular communication systems, a wireless LAN cell only covers several hundreds meters, the range of a hot spot, and supports 10 Mbps to 50 Mbps data rate for each user. Currently, the most popular wireless LAN standard is 802.11b, which can support up to 10 Mbps data rate and has been installed at some hot spots, such as airports, hotels, and campus.

At the same time, other wireless technologies are under intensive study and development, such as Bluetooth, Wireless Personal Area Networks (802.15) and Fixed Broadband Wireless Access Standards (802.16 WirelessMAN).

The rapid progress in the wireless industry, as shown above, requires a better utilization of the limited radio spectrum. This trend has driven the researchers to look for better technologies since the beginning of wireless communications. Some technologies, such as channel coding, modulation and receive diversity, have been extensively studied in the past several decades for efficient information transmissions in the wireless channels. More recently, multiuser detection (MUD), orthogonal frequency division multiplexing (OFDM), and transmit diversity become hot research areas.

1.2 A Brief Review of Diversity

1.2.1 The Concept of Diversity

Wireless channels suffer from fading effects and various diversity techniques are used to relieve the adverse effects. Since most errors occur when the fading distortion is severe, the traditional diversity techniques manage to transmit the same signal L times to decrease the probability of severe fading on all copies of the signal. The repetition could be done in the time domain, frequency domain or space domain [1][4]. Accordingly, these repetition methods are named as time diversity, frequency diversity and space diversity, respectively.

In time diversity, the same signal is transmitted in L time slots. These slots should be separated far enough to make the fading on these slots independent. But if the fading is very slow, i.e. in low mobility or low Doppler frequency situations, the slot separation or interleaving depth will be very large, which incur long delays and is not desirable in such applications as voice.

For frequency diversity, the same signal is transmitted in L frequency carriers simultaneously. The separations between these carriers should be larger than the channel coherence bandwidth to achieve the best diversity performance. Spread spectrum system expands signal bandwidth and uses RAKE receiver to obtain frequency diversity. But when the channel coherence bandwidth is much larger than the signal bandwidth occupied by all carriers, frequency diversity does not exist.

Space diversity uses multiple antennas at receiver/transmitter to combat fading effects. The space between antennas should be sufficiently far apart to make the fading between different antennas independent. Usually, a separation of several

wavelengths at basestations and half wavelength at mobile terminals [5] are required. The commonly used receive diversity employ multiple antennas at the receiver side. Depending on the tradeoff between complexity and performance, the received signal on each antenna can be combined by Switch Combining (SC), Equal Gain Combining (EGC) or Maximum Ratio Combining (MRC). An alternative way is to use differently polarized antennas, called polarization diversity.

However, using multiple antennas at the transmitter side, called transmit diversity, can also greatly improve system capacity. Fig. 1.1 is a general block diagram of space diversity with N transmit antennas and M receive antennas. In modern cellular communications, a base station will serve many mobile terminals, which means the basestation antennas can serve many users. Although the antennas and analog devices are very expensive, the cost of basestations can be shared by multiple users. On the other hand, installing multiple antennas at each mobile terminal is economically unfeasible. What's more, there are strict limits on the size and power consumption of mobile terminals, but antennas are usually large and consume a lot of power. So extensive research work has been carried out on transmit diversity to further improve system throughput.

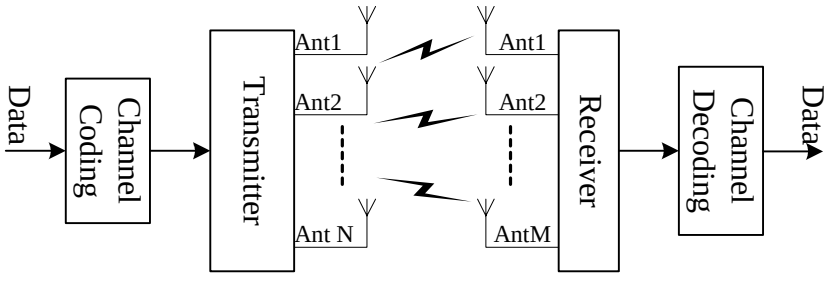

Fig. 1.1 Transmit and receive diversity system.

To prove the benefits that can be gained from transmit diversity, the channel capacity using transmit diversity has been analyzed in the information theoretic

context. Telatar [6] and Foschini [7] showed that the channel capacity can increase linearly with the number of antennas used at each side. Their results are the capacity limit of space diversity in fading channels. How to achieve or approach the theoretical capacity is open to question.

1.2.2 Categories of Transmit Diversity

Current transmit diversity systems fall into 3 categories [8][9]:

I. Schemes using feedback;

II. Those with feedforward or training information but no feedback;

III. Blind schemes.

Schemes in the first category need information of channel that is fed back from the mobiles implicitly or explicitly. In TDD system [10], channel information is implicitly contained in the received signals since the transmitter and receiver use the same frequency. Then the signal to be transmitted can be weighted according to the estimated fading coefficients from the receiver. For FDD systems, the channel information must be sent back from the other side that is usually a mobile terminal. System in [11] uses the feedback to decide which antenna to use. The delay caused by feedback can be a problem if the fading is too fast.

The second category of transmit diversity spreads signal across different antennas using linear processing. The receiver must decode the received signal with such techniques as linear processing, maximum likelihood sequence estimation (MLSE) and equalization. The transmit diversity schemes in [12][13] filter input symbols with a symbol-spaced finite impulse response (FIR) filter prior to modulation. The tap weights of the FIR filter at different antennas are different. They are chosen such that

a necessary condition for optimum diversity gain, i.e. the gain of MRC, in time-selective fading channels is satisfied. The delay diversity scheme, proposed as one of the two schemes in [14], is a special case of [12]. In this scheme, multiple copies of the same signal are transmitted on the different antennas at the different time slots to produce artificial frequency-selective fading. Fig. 1.2 illustrates the linear processing at the transmitter for delay diversity. T is the symbol duration. Hence, equalization or MLSE should be used at the receiver to resolve multipath distortion and obtain diversity from the frequency-selective fading. Results in [15] show that the delay diversity can provide a diversity gain comparable to that of receive diversity.

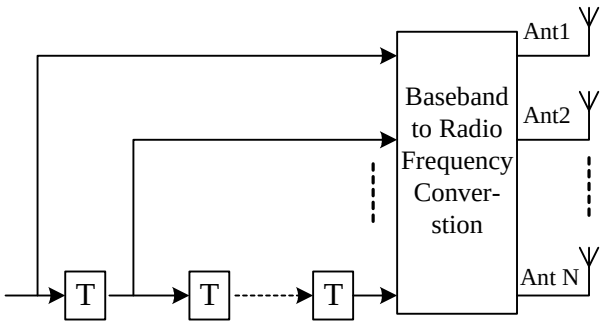

Fig. 1.2 Linear processing at transmitter for delay diversity.

From the coding perspective, delay diversity is a simple repetition code, which is not as efficient as block codes or trellis codes. This observation prompts people to efficiently encode the signals across multiple transmit antennas. Guey et al [16] designed a block code for transmit antennas and better performance was obtained than that of conventional transmit diversity. Soon later, the concept space-time codes (STC) appears. Alamouti [17] found a very simple space-time block code (STBC) for 2 transmit antennas, while Tarokh et al [18] extended STBC to multiple antennas. At the same time, space-time trellis code (STTC) [8] was invented. We will come back to STC in the next section.

The third category of transmit diversity does not require feedback. Multiple transmit antennas are used to cause fast fading [19] or transmit signals in orthogonal manner [14][20][21], which can be done by either time multiplexing, frequency multiplexing, or orthogonal code multiplexing. Channel coding is often employed to correct errors. The scheme in [19] transmits the same signal on all of the antennas, but phase sweepings, which is a small frequency offset, is introduced to each antenna to create artificial fast fading. Error burst caused by fast fading is designed to be within the correction ability of channel coding. One of the 2 schemes in [14] encodes one symbol into N symbols, and transmits the N symbols from N transmit antennas one by one, while other antennas remain silent. Although diversity is obtained by time multiplexing, system throughput is lowered by N times, which is quite undesirable when N is larger. The scheme in [20] divides OFDM subcarriers into N groups and uses each antenna to transmit a group of subcarriers. Diversity is obtained across different groups of subcarriers. Channel coding must be employed across groups of subcarriers to correct the errors on the groups of subcarriers that suffered severe fading. To some extent, the scheme in [21] is an extension to the method in [19]. After applying a specially designed phase shift for each antenna, the CDMA signals are transmitted by multiple antennas simultaneously. This scheme can also be looked upon as using orthogonal codes on different antennas and achieving diversity by orthogonal code multiplexing.

1.3 Space-Time Coding and Its Performances Analysis

Stimulated by various works on transmit diversity, as discussed in the previous section, space-time coding was proposed at the end of the 20^{th} century to exploit the

potential huge capacity of systems composed of multiple transmit antennas and multiple receive antennas, named as multiple input and multiple output (MIMO) systems. Space-time coding contains two subgroups: space-time block code (STBC) [17][18] and space-time trellis code (STTC) [8]. STBC encoder will be introduced in Chapter 3.

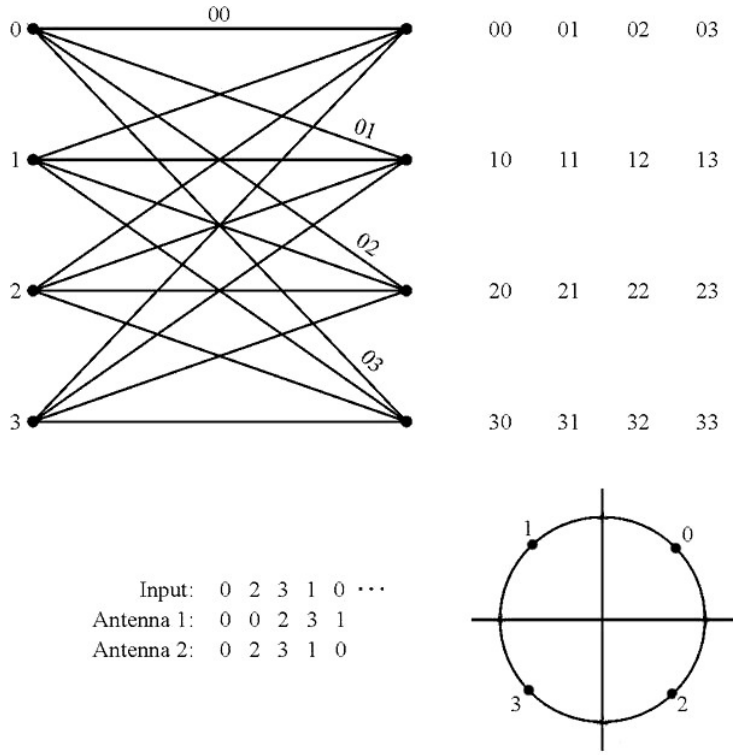

Fig. 1.3 STTC with QPSK, 4 states and 2 transmit antennas [From [4]].

Fig. 1.3 is a simple example of the code construction of STTC with QPSK, 4-state trellis and 2 transmit antennas [4]. The data symbols can be 0, 1, 2, or 3 in QPSK as the constellation shows. For each input data symbol, the trellis output 2 encoded symbols that will be transmitted from 2 transmit antennas simultaneously. The 2 encoded symbols for each state transition branch is listed at the right side of the trellis. Here we assume the initial state is state 0 and data symbol sequence is 02310⋯. Due to the structure of the trellis, the state transition sequence of the encoder

corresponding to the data sequence is also 02310⋯. The code rate of the encoder is 1 and 2 bits are transmitted during each symbol duration.

Although STBC does not have the coding gains of STTC [18], it is still very popular due to its simple decoding algorithms: decoding complexity grows linearly, rather than exponentially as in STTC, with the number of transmit antennas. Alamouti [17] first proposed a 2 transmit antennas STBC along with its decoding algorithm and presented its performance under flat Rayleigh fading channels by simulation. Later, Tarokh et al [18] provided a proof that Alamouti's decoding algorithm is in fact a maximum likelihood (ML) algorithm and found the code construction for any number of transmit antennas under certain optimum criteria. Tarokh et al [22] documented the performance of some STBC schemes in flat Rayleigh fading channels by simulation. Ganesan et al [23] formulated STBC in an optimal signal to noise ratio (SNR) framework. They also derived the distribution of the SNR and closed form expressions for the BER in flat Rayleigh fading channels. Shin et al [24] provided a closed form symbol error probability (SER) expression for STBC over flat Rayleigh fading channels using the equivalent single input single output (SISO) model.

As far as we know, all of these published error rate analyses for STBC are limited to the flat fading case. This is partly due to the inherent difficulty of error rate analysis in frequency-selective fading channels and Rappaport [1] suggests that simulation is the main approach. However, there are still many works devoted to error rate analysis in frequency-selective fading channels, such as Dong et al [25] and Adachi [26]. Both [25] and [26] follow the same approach as that of Bello and Nelin [27][28] in that an error rate expression conditioned on a specific transmitted sequence is first developed, then the final error rate is obtained by averaging over all possible sequences. In their analyses, the systems are assumed to be noise free and the

performance is degraded by ISI. The resultant BER is called average irreducible BER (AIBER), which manifests as an error floor when plotted against SNR for the systems containing noise. This illustrates the impact of ISI over BER performance. In this thesis, we will follow their approach to analyze the AIBER performance of STBC in unequalized frequency-selective fading channels. The result from the above AIBER analysis is the main contribution of the thesis.

Since MLSE is used to decode STTC, pair-wise error probability [29], rather than SER/BER, is analyzed. Tarokh et al [18] and Gong et al [29] analyzed pair-wise error probability of STTC in flat Rayleigh fading channels and frequency-selective Rayleigh fading channels, respectively. This thesis is confined to the study of STBC and will not cover more about STTC.

1.4 Outline of the Thesis

The remainder of the thesis is organized as follows.

In the next chapter, we first examine Wittneben's transmit diversity scheme, one of the pioneering work on transmit diversity. Then, multipath radio propagation phenomenon is illustrated. According to different propagation scenarios, the channels are categorized into flat fading or frequency-selective fading, slow fading or fast fading. Doppler shift, Rayleigh and Ricean distribution are also mentioned. The last part of the chapter proposes a basic STBC system model in flat fading channels and Maximum-likelihood decoding rule for STBC in flat fading channels.

In Chapter 3 we extend the STBC system model in Chapter 2 into frequency-selective fading channels. Here we describe channels in terms of the second order

statistics, namely time frequency correlation function and scattering function. These two functions are simplified using some specific conditions. Then many characteristics of wireless channels can be defined by these functions. One of the most relevant results is the introduction of power delay profiles. Expressions of received signals and decision variables are subsequently derived.

In Chapter 4, we analyze the BER of STBC in flat Rayleigh fading channels. BPSK and QPSK modulations are used. The performance of STBC is compared with that of corresponding receive diversity with Maximum Ration Combing (MRC). The performance curves are plotted at the end of the chapter.

Detailed performance analysis in frequency-selective fading channels, which is the main contribution of the thesis, is presented in Chapter 5. The concept of Average Irreducible Bit Error Rate (AIBER) is firstly introduced. The classic work on general quadratic form is briefly mentioned. Our analysis, which comprises of the following steps, is subsequently performed: first, the characteristic function (CF) of the decision variable is derived following the steps in appendix B of [4]. Then, conditioning the probability of making a wrong decision on a specific transmitted sequence, we transform the CF into a probability density function (PDF) of the decision variable and then derive the BER expression. Finally, the conditional error probability is averaged over all of the possible sequences to obtain the final BER expression.

In Chapter 6, numerical results are presented for the performance analyses in frequency-selective Rayleigh fading channels with rectangular pulse shape and raised cosine pulse shape. We also conduct simulation to verify our analysis. The results show that STBC can effectively suppress fading and ISI, as expected. Some

intermediate variables, such as the second order statistics, are numerically computed to study their properties and verify our previous assumption about these statistics.

In Chapter 7, we provide conclusion for this thesis. Recommendations for future work are also included.

CHAPTER TWO

System and Channel Models

2.1 Introduction

After the background discussion in Chapter 1, here we present the introduction to Wittneben's transmit diversity scheme, Space-time Block Coding (STBC) [17] and Maximum-likelihood (ML) decoding of STBC in flat fading channels. Wireless propagation channel is also studied with the emphasis on physical explanations.

2.2 Wittneben's Transmit Diversity Scheme

Wittneben's transmit diversity scheme [12] is one of the pioneering work on efficient transmit diversity. Here we explain his scheme using two transmit antennas.

This scheme filters input symbols with a symbol-spaced finite impulse response (FIR) filter prior to modulation. For two transmit antennas, we need two FIR filters as shown in Fig. 2.1. $f_{1,v}$ and $f_{2,v}$ are filter weights for antenna 1 and antenna 2, V is the filter order. T is a symbol spaced delay element. The weights should be chosen to meet the criteria

$$\sum_{v} f_{i,v} f_{j,v} = \begin{cases} 1 & \text{for } i = j \\ 0 & \text{otherwise} \end{cases} \tag{2.1}$$

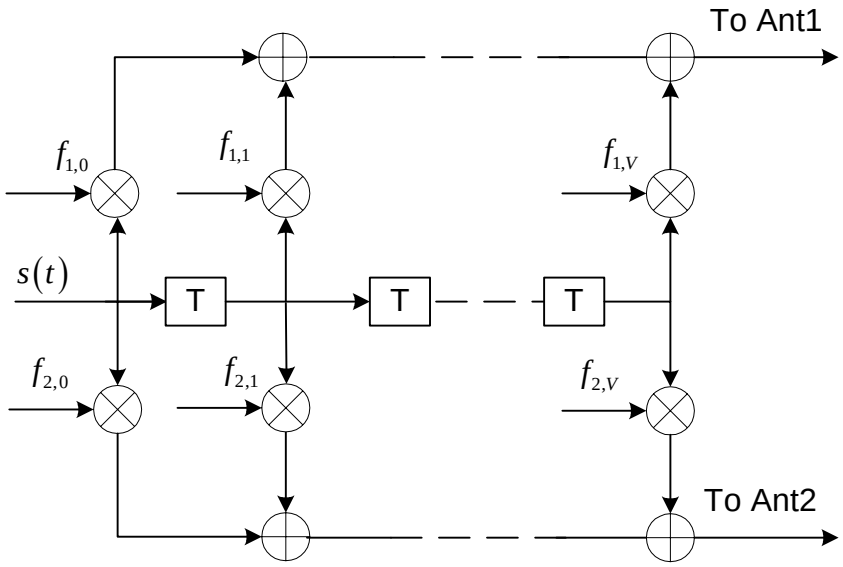

Fig. 2.1 Wittneben's transmit diversity scheme.

Delay diversity is a specific case of this scheme. For example, in the above two-transmit-antenna diversity, we choose filter order 1 and the weights as follows

$$f_{1,0} = 1, \quad f_{1,1} = 0$$
$$f_{2,0} = 0, \quad f_{2,1} = 1$$

Then it becomes delay diversity.

To achieve diversity from this scheme, equalizer must be used to resolve inter-symbol interference (ISI) which is introduced by the FIR filter at the transmitters. As we shall see later, STBC does not incur ISI in the flat fading channels while at the same time STBC achieves full diversity order. This is one of the reasons to explain the popularity of STBC.

2.3 Wireless Channels

2.3.1 Channel Responses

Wireless communication channels are often characterized by severe multipath. Signals from the transmitter propagate along different paths and superpose at the receiver (Fig. 2.2). The different paths are most likely to have different length, so the radio signals on different paths experience different transmission time. This difference results in delay spread at the receiver.

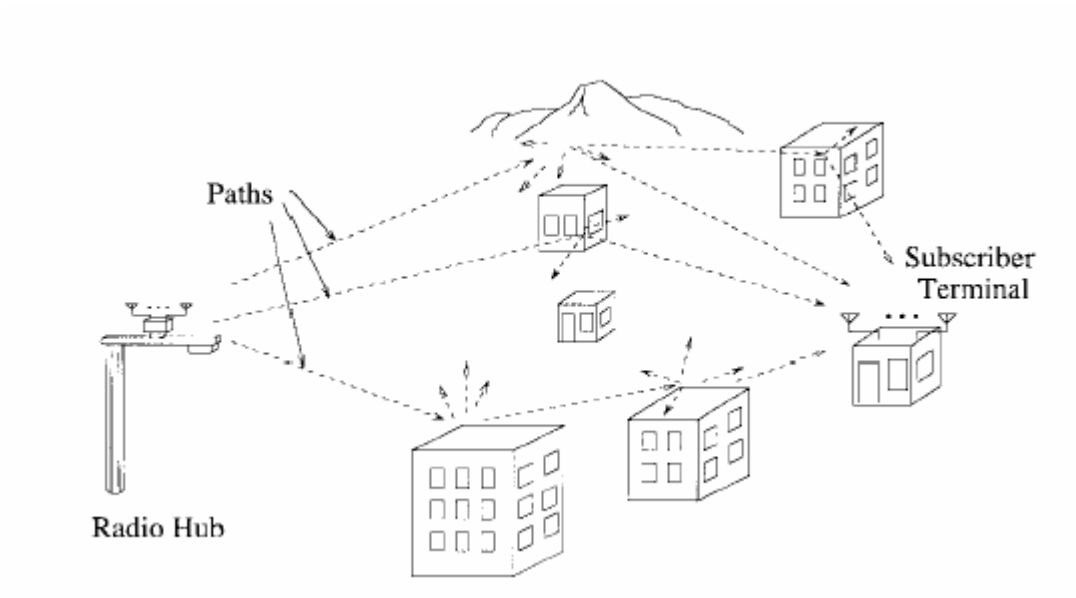

Fig. 2.2 Illustration of the physical wireless channel.

Beyond the delay spread, the wireless channel is also time-variant. As the result of the time-variant characteristic, the channel response to impulses at different time is changing. Fig. 2.3 illustrates both of these two characteristics: delay spread and time-variant.

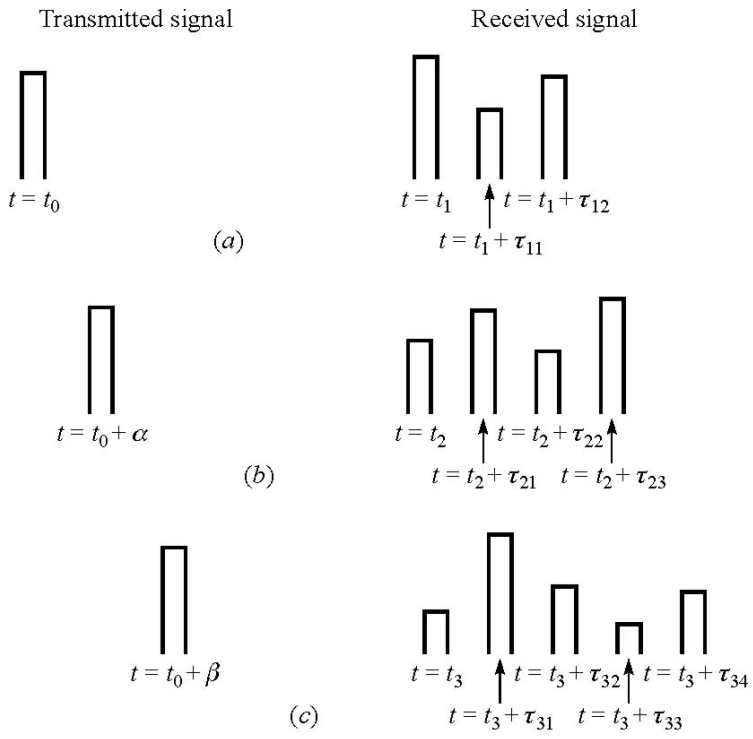

Fig. 2.3 Example of the channel response to an impulse.

We adopt the baseband equivalent signal representation to look for the channel model. If $s(t)$ and $r(t)$ denote the transmitted and received signals, according to Fig. 2.3, the relation between them is

$$r(t) = \sum_n \alpha_n(t) s\left(t - \tau_n(t)\right) \tag{2.2}$$

where $\alpha_n(t)$ is the complex channel fading gains associated with different delays. The envelope of $\alpha_n(t)$ may follow some distributions, such as Rayleigh or Ricean distribution, depending on propagation environment. Then we can separate the channel response from (2.2) as

$$h(t,\tau) = \sum_n \alpha_n(t) \delta\left(t - \tau_n(t)\right) \tag{2.3}$$

$h(t,\tau)$ is the channel response at time t due to an impulse at $t-\tau$. For some channels, it is most appropriate to view the received signal as consisting of a

continuum of multipath components. In this case, the summation in (2.2) should be replaced by integration

$$r(t) = \int_{-\infty}^{\infty} h(t,\tau)s(t-\tau)d\tau \tag{2.4}$$

2.3.2 Flat Fading and Frequency-selective Fading

For flat fading, the channels possess a constant gain and linear phase response over a bandwidth that is greater than the bandwidth of the transmitted signal. Fig. 2.4 illustrates the characteristics of flat fading channel in both of time domain and frequency domain. The spectrum of the transmitted signal is preserved after the channel, although the amplitude is usually changed.

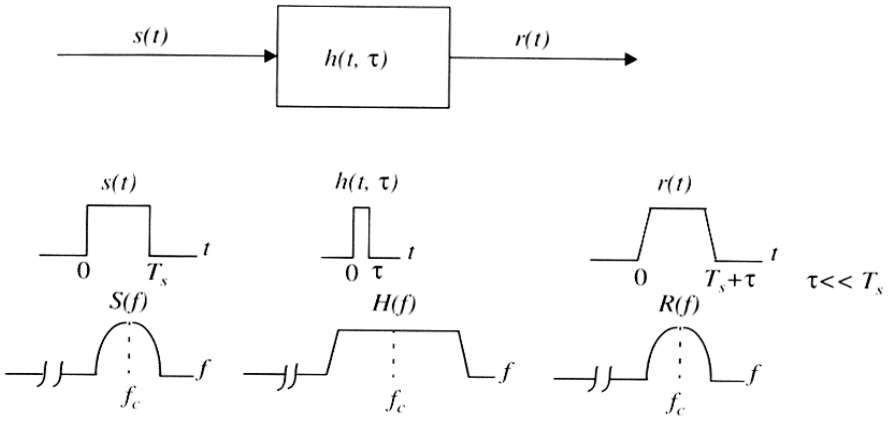

Fig. 2.4 Flat fading channel characteristics [From [1]].

Flat fading channels are suitable channel models for narrow band systems because the bandwidth of the transmitted signal is narrower than the bandwidth of the channels. Since the channels have a wider spectrum than the signal spectrum in frequency domain, the delay spread of the channels in time domain should be much smaller than the reciprocal bandwidth of transmitted signal, or the symbol duration.

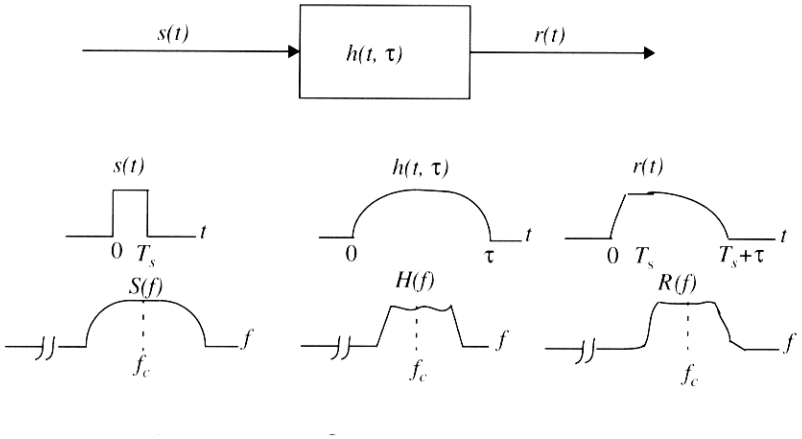

Fig. 2.5 Frequency-selective fading channel characteristics [From [1]].

For frequency-selective fading, the channels have a constant gain and linear phase response over a bandwidth that is smaller than the bandwidth of transmitted signals (Fig. 2.5). Such a condition means the multipath delay spread is greater than the reciprocal bandwidth of transmitted signal, or the symbol duration. When this happens, the received signal contains multiple versions of transmitted signal that are attenuated, delayed in time and thus the received signal is distorted and includes interferences from nearby symbols, the so-called Inter-symbol Interference (ISI). Frequency-selective fading channels are suitable channel models for wideband systems since the signal bandwidth is wider than the bandwidth of channels.

2.3.3 Doppler Shift

Before we discuss fast fading and slow fading, the introduction to Doppler shift should be presented. Consider the scenario in Fig. 2.6: a mobile moving at a constant velocity v along a path segment having length d between points X and Y, while it receives signals from a remote source S. The difference in path lengths traveled by the wave from source S to the mobile at points X and Y is $\Delta l = d\cos\theta = v\Delta t\cos\theta$, where Δt is the time required for the mobile to travel from X to Y, the θ is assumed to be

the same at points X and Y since the source is assumed to be very far away. The phase change in the received signal due to the difference in path lengths is therefore

$$\Delta\phi = \frac{2\pi\Delta l}{\lambda} = \frac{2\pi v\Delta t}{\lambda}\cos\theta \tag{2.5}$$

where λ is radio wave length. The phase change results in frequency change, or Doppler shift

$$f_d = \frac{1}{2\pi\lambda}\frac{\Delta\phi}{\Delta t} = \frac{v}{\lambda}\cos\theta \tag{2.6}$$

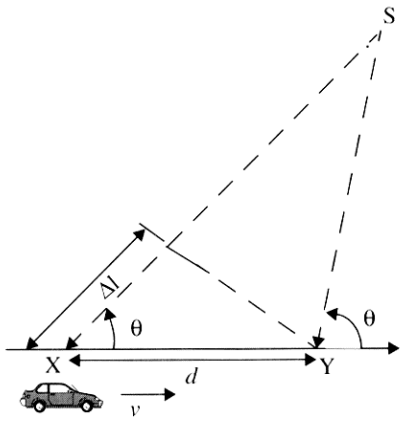

Fig. 2.6 Illustration of Doppler effect.

Since multipath components come from different directions, the Doppler shifts associated with different path are most likely different, which spread the original signal and increase bandwidth. Doppler spread is a measure of the spectral broadening caused by Doppler shifts.

2.3.4 Fast Fading and Slow Fading

Depending on how rapidly the transmitted baseband signal changes as compared to the rate of change of the channel, a channel may be classified either as a fast fading or slow fading channel.

In a fast fading channel, the channel impulse response changes rapidly within the symbol duration. That is, the reciprocal Doppler spread of the channel is smaller than the symbol period of the transmitted signal. This causes frequency dispersion (also called time selective fading) due to Doppler spreading, which leads to signal distortion. Viewed in the frequency domain, signal distortion due to fast fading increase with increasing Doppler spread relative to the bandwidth of the transmitted signal.

In a slow fading channel, the channel impulse response changes at a rate much slower than the transmitted baseband signal. In this case, the channel may be assumed to be static over one or several reciprocal signal bandwidth intervals. In the frequency domain, this implies that the Doppler spread of the channel is much less than the bandwidth of the baseband signal.

It should be noted that when a channel is specified as a fast or slow fading channel, it does not specify whether the channel is flat fading or frequency-selective fading. In practice, fast fading only occurs for very low data rates. In this thesis, we will use both of flat fading and frequency-selective fading channels, but we always assume slow fading.

2.3.5 Rayleigh and Ricean Distribution

The signal amplitude in flat fading channels can suffer deep fades. The distribution of the instantaneous gain of flat fading channels is important for designing radio link.

Rayleigh distribution is commonly used to describe the statistical time varying nature of the received envelope of a fading signal. The envelope of the sum of two quadrature Gaussian noise signals obeys a Rayleigh distribution, which has a probability density function (PDF) given by

$$p(r)=\begin{cases}\dfrac{r}{\sigma^2}\exp\left(-\dfrac{r^2}{2\sigma^2}\right) & for \quad 0\le r\le\infty \\ 0 & for \quad r<0\end{cases} \tag{2.7}$$

where r is the envelope of the received signal and σ^2 is the time-average power of the received signal.

Where there is a dominant nonfading signal component present, such as a line-of-sight propagation path, the fading envelope follows Ricean distribution. In this situation, the random multipath components arriving at different angles are superimposed on the nonfading signal. As the nonfading signal becomes weaker, the envelope of composite signal is close to Rayleigh distributed.

The Ricean distribution is given by

$$p(r)=\begin{cases}\dfrac{r}{\sigma^2}\exp\left(-\dfrac{r^2+A^2}{2\sigma^2}\right)I_0\left(\dfrac{Ar}{\sigma^2}\right) & for \quad 0\le r\le\infty \\ 0 & for \quad r<0\end{cases} \tag{2.8}$$

The parameter A denotes the peak amplitude of the dominant signal and $I_0(\bullet)$ is the modified Bessel function of the first kind and zero order. When A=0, which means the dominant path decreases in amplitude, the Ricean distribution degenerates to a Rayleigh distribution. Fig. 2.7 shows the PDF curves for Ricean distribution, which include Rayleigh distribution as a special case.

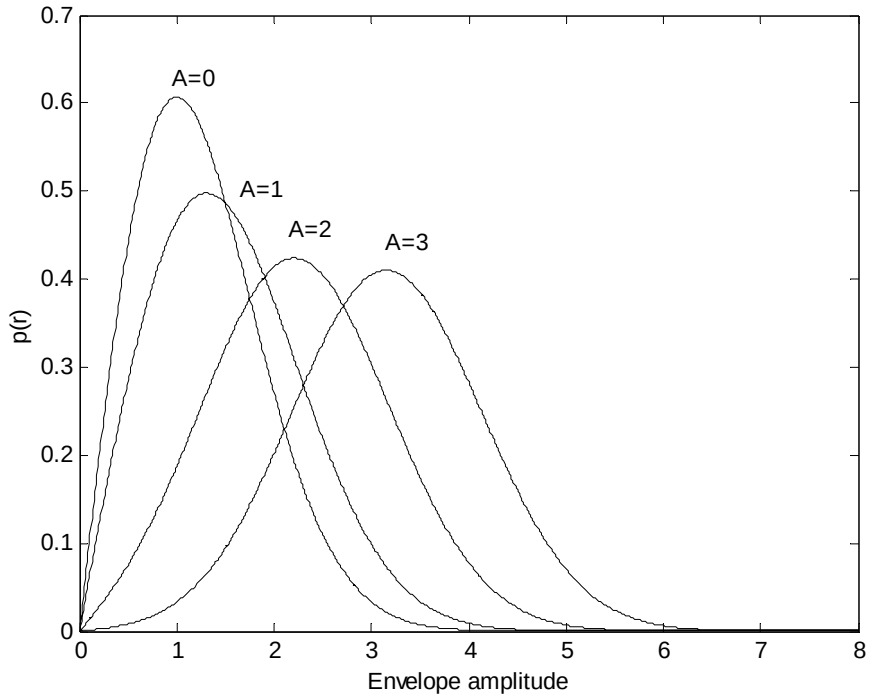

Fig. 2.7 PDF of Rayleigh and Ricean distribution.

The phase of received signal from flat Rayleigh fading channels is evenly distributed phase between $[0, 2\pi)$.

We use the quasi-static channel model in this thesis, which means the channel is static within each code block but changes independently between blocks. For the case of flat Rayleigh fading channels, the fading is simply a complex Gaussian random variable for each coding block.

2.4 STBC System Architecture

Consider a communication system shown in Fig. 2.8 for studying the performance of STBC systems. The data source generates random binary bits. Symbol Mapping converts data bits into symbols. For Binary Phase Shift Keying (BPSK), $\{0,1\}$ are mapped into $\{1,-1\}$. For Quadrature Phase Shift Keying (QPSK), data bits are Gray

encoded: $\{00,01,10,11\}$ are mapped into $\left\{\frac{1}{\sqrt{2}}+\frac{j}{\sqrt{2}},\frac{-1}{\sqrt{2}}+\frac{j}{\sqrt{2}},\frac{1}{\sqrt{2}}-\frac{j}{\sqrt{2}},\frac{-1}{\sqrt{2}}-\frac{j}{\sqrt{2}}\right\}$.

Since we use Alamouti's STBC scheme, the output of STBC coding has 2 branches, one for each antenna.

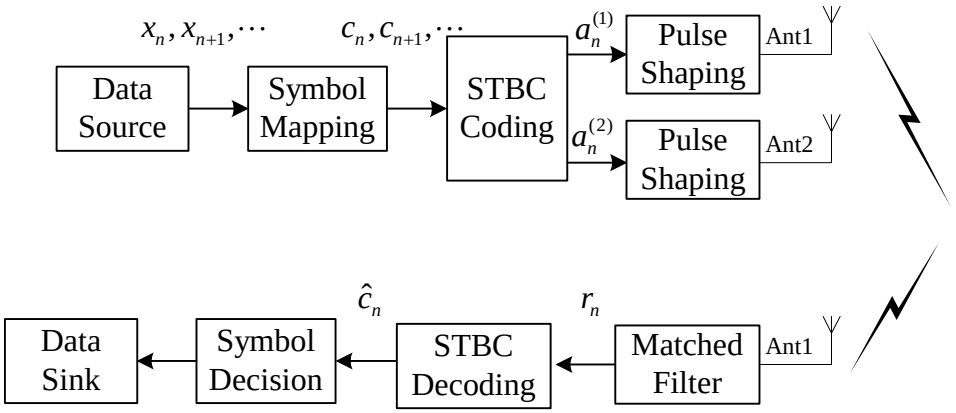

Fig. 2.8 System architecture of the proposed STBC system.

Before radio transmission, a pulse shape should be assigned to each symbol. Let $p_T(t)$ denote the transmit pulse shape and $p_R(t)$ denote the receiver matched filter. Then the combined response is given by

$$p(t) = p_T(t) * p_R(t) \tag{2.9}$$

where * is convolution operation. If $P(f)$, $P_T(f)$ and $P_R(f)$ are the Fourier transforms of corresponding functions, $P(f)$ is usually evenly divided into $P_T(f)$ and $P_R(f)$

$$P_T(f) = P_R(f) = \sqrt{P(f)} \tag{2.10}$$

Two commonly used impulse responses are

$$p(t)=\frac{\sin(\pi t/T)}{\pi t/T}\frac{\cos(\alpha\pi t/T)}{1-(2\alpha t/T)^2} \tag{2.11}$$

for raised cosine (RC) pulse shaping and

$$p(t)=\begin{cases}1-\dfrac{|t|}{T}, & if\ |t|\le T\\ 0, & elsewhere\end{cases} \tag{2.12}$$

for rectangular pulse shaping.

2.5 Space-time Block Coding

Consider a STBC system with two transmit antennas and one receive antenna. Assuming symbol *n* and *n+1* is the STBC coding block in Alamouti's [17] scheme. The original symbol sequence $c_n, n=\cdots,n-1,n,n+1,\cdots$ is encoded into $a_n^{(i)}, i=1,2; n=\cdots,n-1,n,n+1,\cdots$, which are transmitted on antenna i at time n:

$$\begin{cases}a_n^{(1)}=c_n\\ a_n^{(2)}=c_{n+1}\\ a_{n+1}^{(1)}=-c_{n+1}^*\\ a_{n+1}^{(2)}=c_n^*\end{cases} \tag{2.13}$$

In Fig. 2.9, we show the code construction.

Ant1	$-c_{n-1}^*$	c_n	$-c_{n+1}^*$	c_{n+2}
	$a_{n-1}^{(1)}$	$a_n^{(1)}$	$a_{n+1}^{(1)}$	$a_{n+2}^{(1)}$
Ant2	c_{n-2}^*	c_{n+1}	c_n^*	c_{n+3}
	$a_{n-1}^{(2)}$	$a_n^{(2)}$	$a_{n+1}^{(2)}$	$a_{n+2}^{(2)}$

Fig. 2.9 The structure of Alamouti's STBC.

The transmitted signal from antenna i can be expressed as

$$s^{(i)}(t) = \sum_{l} \sqrt{\frac{E_s}{2}} a_l^{(i)} p_T(t - lT) \tag{2.14}$$

where $p_T(t)$ is transmitter filter impulse response to shape the signal, $a_l^{(i)}$ is the STBC encoded symbols. $E_s = P_S T$ is symbol energy, where the total transmitted power P_S is equally distributed to 2 antennas. So the symbol energy on each antenna is $\frac{E_s}{2}$. After matched filtering, the received signals is:

$$r(t) = \sum_{i=1}^{2} s^{(i)}(t) * h^{(i)} * p_R(t) + w(t) \tag{2.15}$$

Then sampling $r(t)$ at time *nT*:

$$\begin{aligned} r_n &= \sum_{i=1}^{2} \sum_{l} \sqrt{\frac{E_s}{2}} a_l^{(i)} p(nT - lT) h^{(i)} + w_n \\ &= \sum_{i=1}^{2} \sqrt{\frac{E_s}{2}} a_n^{(i)} h^{(i)} + w_n \end{aligned} \tag{2.16}$$

where $h^{(i)}, i = 1,2$ denote the fading coefficients between 2 transmit and 1 receive antennas. In the above derivation, $p(nT - lT) = 0 \quad for \quad n \neq l$, which means there does not exist ISI. $w_n = w_{n,r} + j w_{n,i}$ is a complex noise component with $\frac{1}{2} E\left[w_n w_n^* \right] = \frac{N_0}{2}$. The received signals at time *n* and *n+1* can be written as

$$\begin{cases} r_n = \sqrt{\frac{E_s}{2}} h^{(1)} a_n^{(1)} + \sqrt{\frac{E_s}{2}} h^{(2)} a_n^{(2)} + w_n \\ r_{n+1} = \sqrt{\frac{E_s}{2}} h^{(1)} a_{n+1}^{(1)} + \sqrt{\frac{E_s}{2}} h^{(2)} a_{n+1}^{(2)} + w_{n+1} \end{cases} \tag{2.17}$$

2.6 Maximum-likelihood Decoding

According to STBC coding rule, (2.17) can be written into

$$\begin{cases} r_n = \sqrt{\frac{E_s}{2}} h^{(1)} c_n + \sqrt{\frac{E_s}{2}} h^{(2)} c_{n+1} + w_n \\ r_{n+1} = -\sqrt{\frac{E_s}{2}} h^{(1)} c_{n+1}^* + \sqrt{\frac{E_s}{2}} h^{(2)} c_n^* + w_{n+1} \end{cases} \tag{2.18}$$

Since in the thesis, only one receive antenna is used, the ML decoding is simply to minimize

$$\left| r_n - \sqrt{\frac{E_s}{2}} h^{(1)} c_n - \sqrt{\frac{E_s}{2}} h^{(2)} c_{n+1} \right|^2 + \left| r_{n+1} + \sqrt{\frac{E_s}{2}} h^{(1)} c_{n+1}^* - \sqrt{\frac{E_s}{2}} h^{(2)} c_n^* \right|^2 \tag{2.19}$$

over all possible values of c_n and c_{n+1}. The extension to multiple receive antennas is straightforward. We expand the above expression

$$\begin{aligned} & |r_n|^2 + |r_{n+1}|^2 \\ & + \frac{E_s}{2}\left(|h^{(1)}|^2 + |h^{(2)}|^2 \right) |c_n|^2 - \sqrt{\frac{E_s}{2}} c_n^* \left(r_n h^{(1)*} + r_{n+1}^* h^{(2)} \right) - \sqrt{\frac{E_s}{2}} c_n \left(r_n^* h^{(1)} + r_{n+1} h^{(2)*} \right) \\ & + \frac{E_s}{2}\left(|h^{(1)}|^2 + |h^{(2)}|^2 \right) |c_{n+1}|^2 - \sqrt{\frac{E_s}{2}} c_{n+1}^* \left(r_n h^{(2)*} - r_{n+1}^* h^{(1)} \right) - \sqrt{\frac{E_s}{2}} c_{n+1} \left(r_n^* h^{(2)} - r_{n+1} h^{(1)*} \right) \end{aligned} \tag{2.20}$$

Clearly, the first two terms, $|r_n|^2 + |r_{n+1}|^2$ is independent of code words and can be neglected. What's more, (2.20) can be divided into two parts: one part is the second row, which is only a function of c_n; the other part is the third row, which is only a function of c_{n+1}. Thus the minimization of (2.20) is equivalent to minimize these two parts independently.

For the first part, $\left|r_n h^{(1)*} + r_{n+1}^* h^{(2)}\right|^2$ can be appended since it is independent of c_n. Then the first part can be written as

$$\left|\left(r_n h^{(1)} + r_{n+1}^* h^{(2)}\right) - \sqrt{\frac{E_s}{2}} c_n\right|^2 + \frac{E_s}{2}\left(-1 + \left(\left|h^{(1)}\right|^2 + \left|h^{(2)}\right|^2\right)\right)\left|c_n\right|^2 \tag{2.21}$$

Similarly, the second part can be written as

$$\left|\left(r_n h^{(2)*} - r_{n+1}^* h^{(1)}\right) - \sqrt{\frac{E_s}{2}} c_{n+1}\right|^2 + \frac{E_s}{2}\left(-1 + \left(\left|h^{(1)}\right|^2 + \left|h^{(2)}\right|^2\right)\right)\left|c_{n+1}\right|^2 \tag{2.22}$$

When all symbols have the same energy, i.e. $\left|c_n\right|^2 = \left|c_{n+1}\right|^2$, the second terms in (2.21) and (2.22) can be deleted. Then, the final ML decoding method is

$$\begin{cases} \hat{c}_n = r_n h^{(1)} + r_{n+1}^* h^{(2)} \\ \hat{c}_{n+1} = r_n h^{(2)*} - r_{n+1}^* h^{(1)} \end{cases} \tag{2.23}$$

We shall use (2.23) as our decoding method in Chapter 4 and Chapter 5.

CHAPTER THREE

STBC in Frequency-selective Fading Channels

3.1 Introduction

With the basic model of STBC in Chapter 2, here we extend it to incorporate the effects of more complex frequency-selective fading channels. We begin this Chapter with the introduction of the second order statistics of channels. Compared with the channel introduction in Chapter 2, which explain the channel properties with the emphasis on physical meanings, here we mainly describe wireless channels using the second order statistics. Then the frequency-selective fading channel model is incorporated into our previous STBC system. Finally, decoding rule in the frequency-selective fading channels is investigated.

3.2 The Second Order Statistics of Channels

3.2.1 Power Delay Profile

Due to the difficulty to fully describe the statistics of randomly time-variant linear channels, the second order statistics, specifically, the autocorrelation functions, are

investigated. Let $h(t,\tau)$ denote the channel impulse response at time t due to an impulse at time $t-\tau$, the autocorrelation function of the channel impulse response is defined as

$$R_h(t_1,t_2;\tau_1,\tau_2)=\frac{1}{2}E\left[h(t_1,\tau_1)h^*(t_2,\tau_2)\right] \tag{3.1}$$

To further the development of the above expression, we need two assumptions. Firstly, the channel is wide-sense-stationary (WSS), which means the autocorrelation function only depends on the time interval $\Delta t=t_1-t_2$, rather than their specific time t_1 and t_2. Secondly, channel gains associated with different path delays are uncorrelated. In other words, different scatterers are uncorrelated (US). Most practical wireless channels meet the requirements of these two conditions ([30]). Then, the channel is wide-sense-stationary uncorrelated scattering (WSSUS) and the autocorrelation function becomes

$$\frac{1}{2}E\left[h(t_1,\tau_1)h^*(t_2,\tau_2)\right]=R_h(\Delta t;\tau_1)\delta(\tau_1-\tau_2) \tag{3.2}$$

where $\delta(t)$ is Dirac delta function. When we set $\Delta t=0$, $R_h(0;\tau)\equiv R_h(\tau)$. $R_h(\tau)$ is the average power output of the channel as a function of the time delay τ and called power delay profile (PDP), or multipath intensity profile. The area under $R_h(\tau)$ is commonly normalized to 1.

Root mean square (RMS) delay spread τ_{rms} is defined as [30]:

$$\tau_{mean}=\int_{-\infty}^{\infty}\tau R_h(\tau)d\tau \tag{3.3}$$

$$\tau_{rms}=\sqrt{\int_{-\infty}^{\infty}\left(\tau-\tau_{mean}\right)^2 R_h(\tau)d\tau} \tag{3.4}$$

In [28], [31] and [32], it is shown that the error rate performance of digital modulation systems has a strong relation with τ_{rms}. Without loss of generality, we assume $\tau_{mean} = 0$ and the sampling time is locked to τ_{mean}.

Commonly used power delay profiles are [25]:

1) Double-spike profile

$$R_h(\tau) = \frac{1}{2}\delta(\tau - \tau_{rms}) + \frac{1}{2}\delta(\tau + \tau_{rms}) \tag{3.5}$$

2) Gaussian profile

$$R_h(\tau) = \frac{1}{\sqrt{2\pi}\tau_{rms}} \exp\left(-\frac{\tau^2}{2\tau_{rms}^2}\right) \tag{3.6}$$

3) One-sided exponential profile

$$R_h(\tau) = \begin{cases} \frac{1}{\tau_{rms}} \exp\left(-\frac{\tau + \tau_{rms}}{\tau_{rms}}\right) & if \quad \tau \geq -\tau_{rms} \\ 0 \quad elsewhere \end{cases} \tag{3.7}$$

Fig. 3.1 shows the shape of the three PDP.

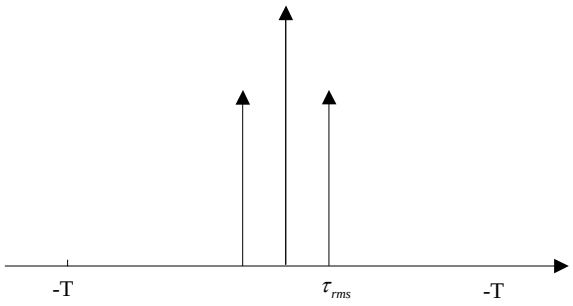

(a)

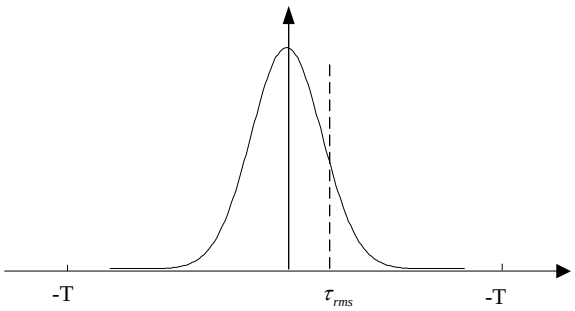

(b)

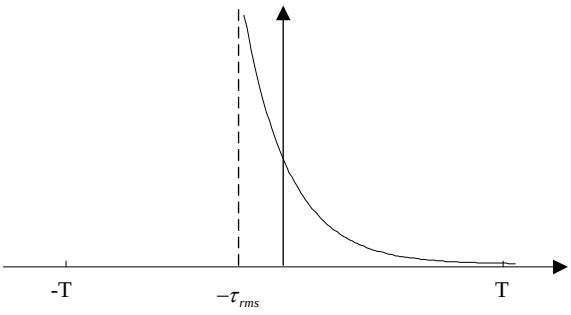

(c)

Fig. 3.1 (a) Double-spike profile, (b) Gaussian profile and (c) one-sided exponential profile.

If the fading is flat, we can drop τ in $h(t,\tau)$. PDP becomes one impulse $\delta(\tau)$ and $\tau_{rms}=0$.

3.2.2 Time Frequency Correlation Function

A complete analogous characterization of the time-variant multipath channel can be performed in the frequency domain. The time-variant transfer function $T(f,t)$ is obtained by taking Fourier transform of $h(t,\tau)$

$$T(f,t)=\int_{-\infty}^{+\infty}h(t,\tau)\exp(-j2\pi f\tau)d\tau \tag{3.8}$$

If $h(t,\tau)$ is modeled as a complex value zero mean Gaussian random process in the *t* variable, then after the linear transformation in (3.8), $T(f,t)$ is also a complex value zero mean Gaussian random process. Under the assumption that the channel is wide-sense-stationary, we define the autocorrelation function

$$R_T(f_1,f_2;\Delta t)=\frac{1}{2}E\left[T(f_1,t_1)T^*(f_2,t_2)\right] \tag{3.9}$$

Substituting (3.8) into (3.9), it is straightforward to establish the relation between $R_h(\Delta t;\tau_1)$ and $R_T(f_1,f_2;\Delta t)$

$$\begin{aligned}
R_T(f_1,f_2;\Delta t)&=\int_{-\infty}^{+\infty}\int_{-\infty}^{+\infty}\frac{1}{2}E\left[h(t_1,\tau_1)h^*(t_2,\tau_2)\right]\exp(j2\pi(f_2\tau_2-f_1\tau_1))d\tau_1d\tau_2\\
&=\int_{-\infty}^{+\infty}\int_{-\infty}^{+\infty}R_h(\Delta t;\tau_1)\delta(\tau_1-\tau_2)\exp(j2\pi(f_2\tau_2-f_1\tau_1))d\tau_1d\tau_2\\
&=\int_{-\infty}^{+\infty}R_h(\Delta t;\tau_1)\exp(j2\pi(f_2-f_1)\tau_1)d\tau_1\\
&=\int_{-\infty}^{+\infty}R_h(\Delta t;\tau_1)\exp(-j2\pi\Delta f\tau_1)d\tau_1\\
&\equiv R_T(\Delta f;\Delta t)
\end{aligned} \tag{3.10}$$

where $\Delta f = f_1 - f_2$. (3.10) shows $R_T(\Delta f;\Delta t)$ is the Fourier transform of $R_h(\Delta t;\tau)$ on the variable τ. Furthermore, the assumption of uncorrelated scattering implies that the autocorrelation function of $T(f,t)$ in frequency is a function of only the frequency difference $\Delta f = f_1 - f_2$. Therefore, $R_T(\Delta f;\Delta t)$ is called time frequency correlation function ([30]).

Suppose we set $\Delta t = 0$ in (3.10). Then with $R_T(\Delta f;0) \equiv R_T(\Delta f)$, the transform relationship is

$$R_T(\Delta f) = \int_{-\infty}^{+\infty} R_h(\tau)\exp\left(-j2\pi\Delta f\tau\right)d\tau \tag{3.11}$$

Fig. 3.2 depicts the relationship. Since $R_T(\Delta f)$ is an autocorrelation function in the frequency variable, it provides us with a measure of the frequency coherence of the channel. As a result of the Fourier transform relationship between $R_T(\Delta f)$ and $R_h(\tau)$, the reciprocal of the multipath spreads is a measure of the coherence bandwidth of the channel

$$(\Delta f)_c = \frac{1}{T_m} \tag{3.12}$$

where $(\Delta f)_c$ denotes coherence bandwidth, T_m denotes multipath delay spread that is the range of the values of τ over which $R_h(\tau)$ is essentially none zero. Two sinusoids with frequency separation greater than $(\Delta f)_c$ are affected differently by the channel. Therefore, for frequency-selective fading, the bandwidth of signal is larger than $(\Delta f)_c$ and signal is severely distorted by the channel. For flat fading, the bandwidth of signal is smaller than $(\Delta f)_c$.

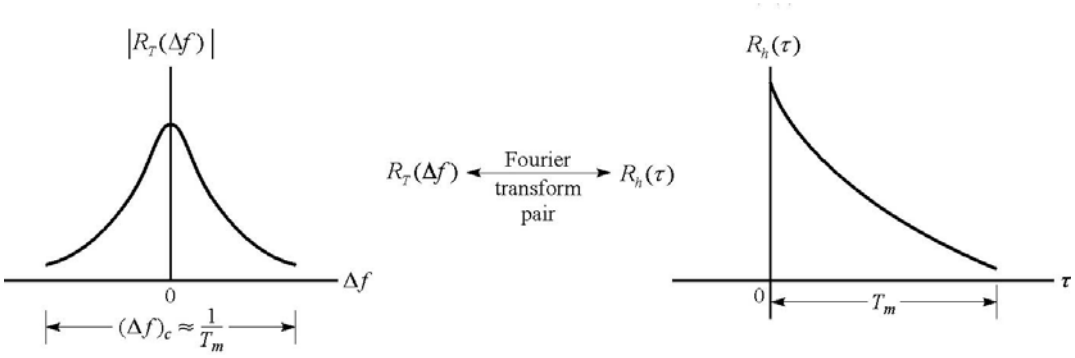

Fig. 3.2 Relationship between $R_T(\Delta f)$ and $R_h(\tau)$

3.2.3 Scattering Function

A simple way to derive scattering function is by the double Fourier transform

$$R_S(\tau;\lambda) = \int_{-\infty}^{+\infty}\int_{-\infty}^{+\infty} R_T(\Delta f;\Delta t)\exp\left(j2\pi\lambda\Delta t\right)\exp\left(j2\pi\tau\Delta f\right)d\Delta t d\Delta f \qquad (3.13)$$

It provides us with a measure of the average power output of the channel as a function of time delay τ and the Doppler frequency λ. Fig. 3.3 illustrates the scattering function of a tropospheric scatter channel, where the scale unit for delay is 0.1 microsecond (*us*) and the scale ranges from 1 to 10. From the graph, we observe that multipath spread $T_m \approx 0.7\,us$. On the other hand, the Doppler spread, which may be defined as the largest of 3-dB bandwidth of the power spectrum, is several hertz.

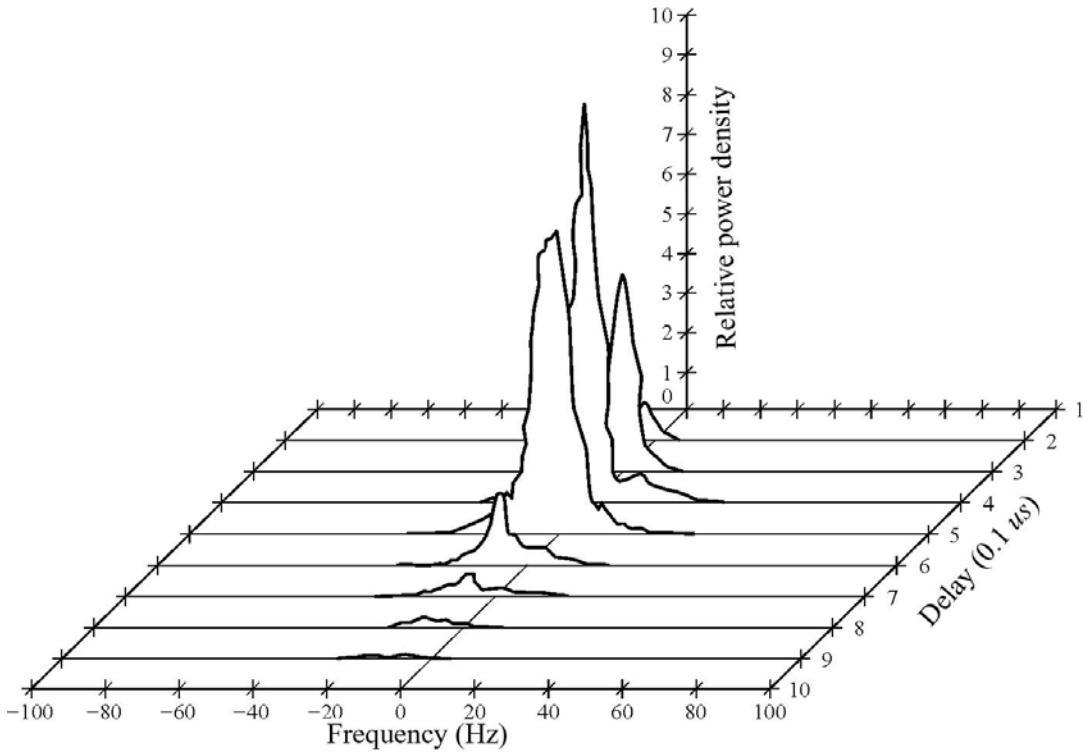

Fig. 3.3 A typical scattering function.

To better observe the time variation in the channel, we integrate $R_S(\tau;\lambda)$ along the variable τ

$$\int_{-\infty}^{+\infty} R_S(\tau;\lambda)\, d\tau \equiv R_S(\lambda) \tag{3.14}$$

The function $R_S(\lambda)$ is a power spectrum that gives the signal intensity as a function of the Doppler frequency λ. Thus we call $R_S(\lambda)$ the Doppler power spectrum. Doppler spread B_d is the range of the values of λ over which $R_S(\lambda)$ is essentially none zero. Since $R_S(\lambda)$ is related to $R_T(\Delta t)$ by the Fourier transform, the reciprocal of B_d is a measure of the coherence time of the channel

$$(\Delta t)_c \approx \frac{1}{B_d} \tag{3.15}$$

where $(\Delta t)_c$ denotes the coherence time. Clearly, a slowly changing channel has a large coherence time or, equivalently, a small Doppler spread. If the bandwidth of transmitted signal is much greater than Doppler spread, the channel is slow fading. Fig. 3.4 illustrates the relationship between $R_T(\Delta t)$ and $R_S(\lambda)$. In our work, the channel is quasi-static, which belongs to slow fading.

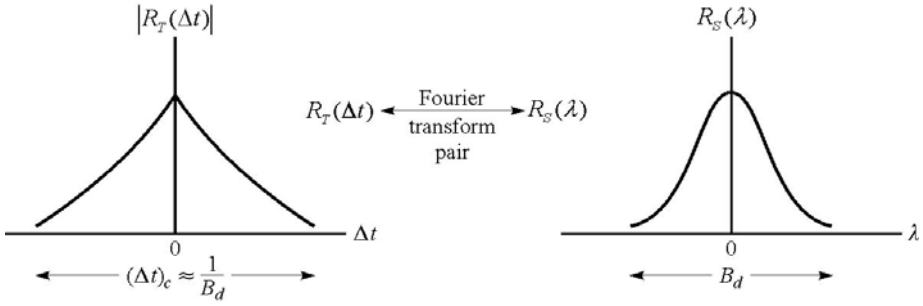

Fig. 3.4 Relationship between $R_T(\Delta t)$ and $R_S(\lambda)$.

Finally, the relationships between time frequency correlation function $R_T(\Delta f;\Delta t)$ and scattering function $R_S(\tau;\lambda)$ is summarized in Fig. 3.5. This figure also shows that $R_T(\Delta t)$ and $R_T(\Delta f)$ are derived from $R_T(\Delta f;\Delta t)$ by setting $\Delta f = 0$ and $\Delta t = 0$, $R_S(\lambda)$ and $R_h(\tau)$ are derived from $R_S(\tau;\lambda)$ by $\int R_S(\tau;\lambda)d\tau$ and $\int R_S(\tau;\lambda)d\lambda$. Bello [30] provides a more complete presentation of the relationships among the channel functions and the second order statistics.

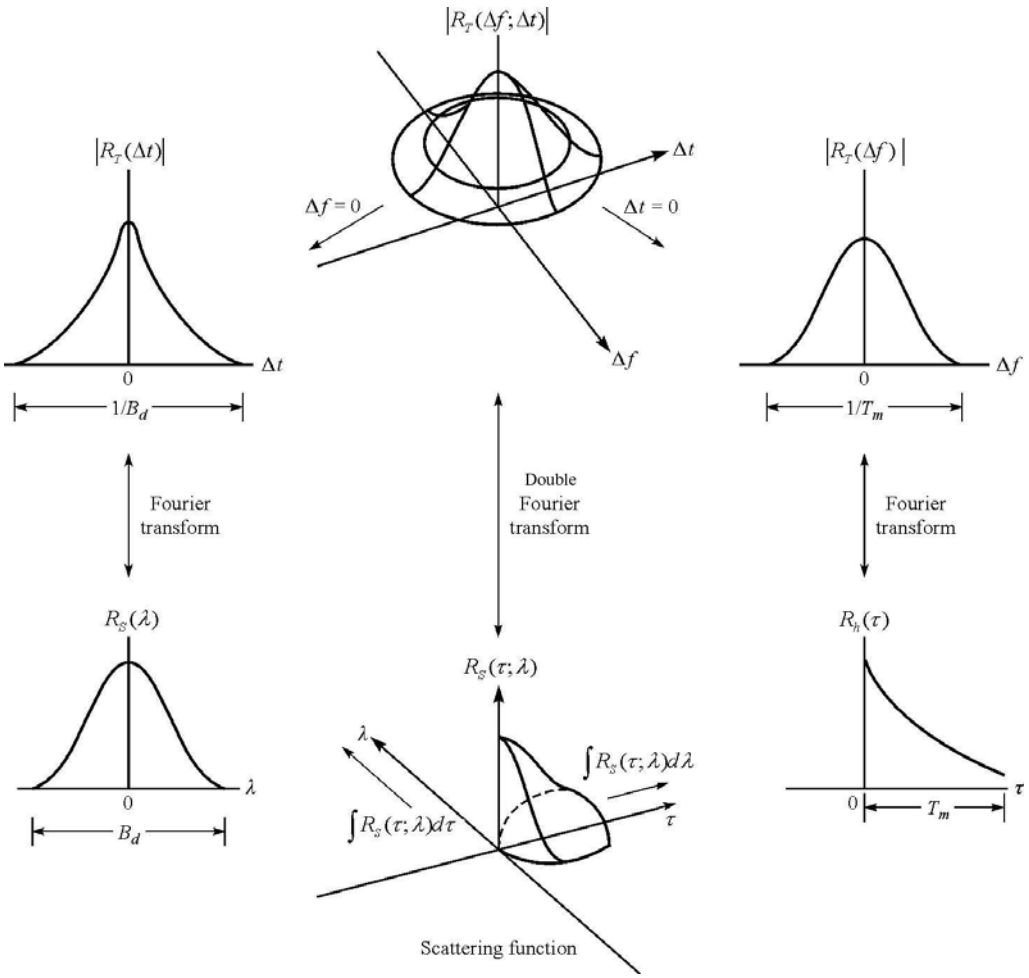

Fig. 3.5 Relationships among channel correlation function [From [4]].

3.3 Decoding in Frequency-selective Fading Channels

Incorporating the frequency-selective fading channel model $h(t,\tau)$, Dong et. al. [25] first developed an expression with integrals to describe the received signals. Adachi [26] elaborated the expression later. With this expression, it is convenient to find error probabilities using the second order statistics of the channel. Following their model, (2.15) should be re-derived as

$$\begin{aligned} r(t) &= \sum_{i=1}^{2} s^{(i)}(t) * h^{(i)}(t,\tau) * p_R(t) + w(t) \\ &= \sum_{i=1}^{2}\sum_{l} \sqrt{\frac{E_s}{2}} a_l^{(i)} p(t-lT) * h^{(i)}(t,\tau) + w(t) \\ &= \sum_{i=1}^{2}\sum_{l} \sqrt{\frac{E_s}{2}} a_l^{(i)} \int_{-\infty}^{\infty} p(t-lT-\tau) h^{(i)}(t,\tau) d\tau + w(t) \end{aligned} \tag{3.16}$$

Sampling received signal $r(t)$ at time $t = nT$:

$$\begin{aligned} r_n &= \sum_{i=1}^{2}\sum_{l} \sqrt{\frac{E_s}{2}} a_l^{(i)} \int_{-\infty}^{\infty} p(nT-lT-\tau) h^{(i)}(t=nT,\tau) d\tau + w_n \\ &= \sum_{i=1}^{2}\sum_{m} \sqrt{\frac{E_s}{2}} a_{n-m}^{(i)} \int_{-\infty}^{\infty} p(mT-\tau) h^{(i)}(t=nT,\tau) d\tau + w_n \\ &= \sum_{i=1}^{2}\sum_{m} \sqrt{\frac{E_s}{2}} a_{n-m}^{(i)} d_m^{(i)} + w_n \end{aligned} \tag{3.17}$$

where

$$m = n - l \tag{3.18}$$

$$d_m^{(i)} = \int_{-\infty}^{\infty} p(mT-\tau) h^{(i)}(t=nT,\tau) d\tau \tag{3.19}$$

$d_m^{(i)}$ is the composite impulse response of transmitter/receiver filter and multipath channel for transmit antenna i. The index m represents symbol shifts. $m = 0$ means response from the current symbol, $m = 1$ means response from the previous symbol, $m = -1$ means response from the following symbol. Most of received signal energy will be contained in $d_0^{(i)}$ as long as the RMS delay spread is small when compared to the symbol duration, which is the case we are interested in (Since equalization is not used, RMS delay spread cannot be larger than half symbol). If we know the multipath channel impulse response, $d_0^{(i)}$ is recovered as channel estimates for the current

symbol. $w_n = w_{n,r} + jw_{n,i}$ is a complex noise component with $\frac{1}{2}E\left[w_n w_n^*\right] = \frac{N_0}{2}$. The received signals at time *n* and *n+1* can be written as

$$\begin{cases} r_n = \sum_{m=-\infty}^{+\infty} \sqrt{\frac{E_s}{2}} a_{n-m}^{(1)} d_m^{(1)} + \sum_{m=-\infty}^{+\infty} \sqrt{\frac{E_s}{2}} a_{n-m}^{(2)} d_m^{(2)} + w_n \\ r_{n+1} = \sum_{m=-\infty}^{+\infty} \sqrt{\frac{E_s}{2}} a_{n-m+1}^{(1)} d_m^{(1)} + \sum_{m=-\infty}^{+\infty} \sqrt{\frac{E_s}{2}} a_{n-m+1}^{(2)} d_m^{(2)} + w_{n+1} \end{cases} \tag{3.20}$$

Since we assume the RMS delay spread is small, say less than half of the symbol duration, only the immediate adjacent symbols at each side need to be considered. So *m* can be set to $m \in \{-1, 0, 1\}$:

$$\begin{cases} r_n = \sum_{m=-1,0,1} \sqrt{\frac{E_s}{2}} a_{n-m}^{(1)} d_m^{(1)} + \sum_{m=-1,0,1} \sqrt{\frac{E_s}{2}} a_{n-m}^{(2)} d_m^{(2)} + w_n \\ r_{n+1} = \sum_{m=-1,0,1} \sqrt{\frac{E_s}{2}} a_{n-m+1}^{(1)} d_m^{(1)} + \sum_{m=-1,0,1} \sqrt{\frac{E_s}{2}} a_{n-m+1}^{(2)} d_m^{(2)} + w_{n+1} \end{cases} \tag{3.21}$$

Numerical results in Chapter 6 corroborate the appropriateness of this approximation. The interferences from the symbols further than the adjacent symbols are practically negligible.

To help illustrate the structure of r_n, we use a rectangular pulse shape (2.12) and double-spike PDP (3.5) as an example. Since we use a quasi-static channel model, the channel fading gains remain constant during one coding block. So we can drop the time *t* in the channel impulse response

$$h^{(i)}(\tau) = h_1^{(i)} \delta(\tau - \tau_{rms}) + h_2^{(i)} \delta(\tau + \tau_{rms}) \tag{3.22}$$

The normalized RMS delay spread *d* is defined as

$$d = \frac{\tau_{rms}}{T} \tag{3.23}$$

Assuming d to be within $[0, 0.5)$. We can find the expressions for $d_m^{(i)}$

$$d_0^{(i)} = (1-d)(h_1^{(i)} + h_2^{(i)}) \tag{3.24}$$

and

$$d_{\pm 1}^{(i)} = d(h_1^{(i)} + h_2^{(i)}) \tag{3.25}$$

In this case, the received signals can be illustrated as in Fig. 3.6.

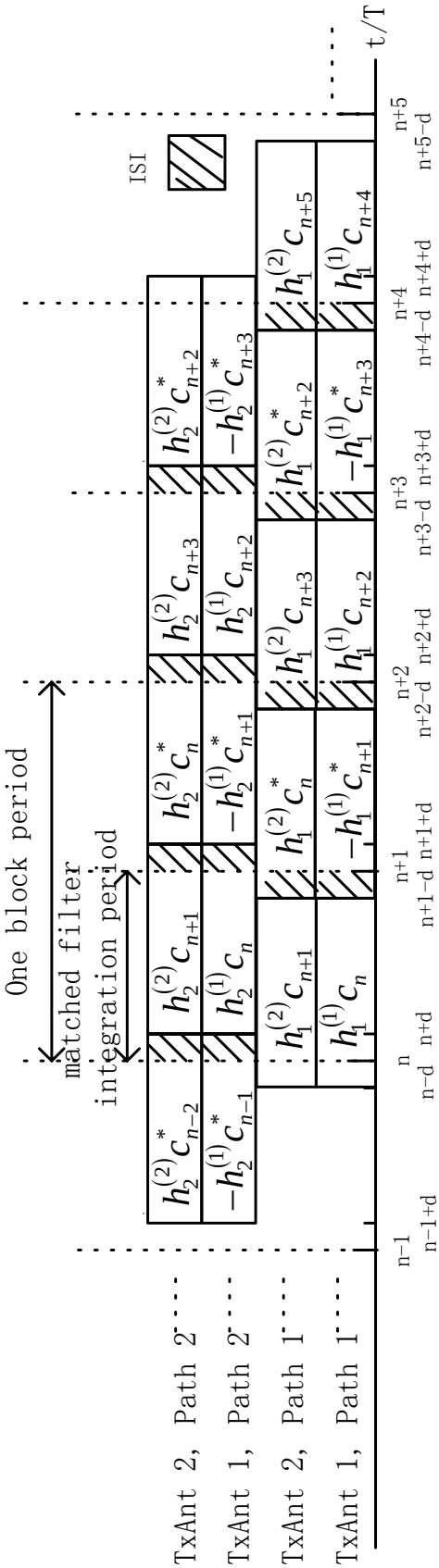

Fig. 3.6 Illustration of the received signals using double-spike PDP.

Using $d_0^{(i)}$ as channel estimates, the decision metric is [17]

$$\begin{cases} \hat{c}_n = r_n d_0^{(1)*} + r_{n+1}^* d_0^{(2)} \\ \hat{c}_{n+1} = r_n d_0^{(2)*} - r_{n+1}^* d_0^{(1)} \end{cases} \tag{3.26}$$

In the flat fading channels, Tarokh et al [22] has shown that (3.26) is a ML decoding rule, as we have shown in Chapter 2. Essentially, the estimate $\hat{c}_n$ is obtained by summing the output of the matched filter, weighted by the associated fading gains, spanning two symbol durations on *nT* and *(n+1)T*. But in the frequency-selective fading channels, if no equalization is employed, $\hat{c}_n$ and $\hat{c}_{n+1}$ contain interferences from the other symbols (ISI) that can be seen from Fig. 3.6. Therefore, the maximum likelihood sequence estimate (MLSE) algorithm will achieve the best BER performance. However, the complexity of MLSE will grow exponentially with the increase of ISI terms. Therefore, we retain the use of (3.26) in our error probability performance analysis in Chapter 5.

CHAPTER FOUR

Performance Analysis in Flat Rayleigh Fading Channels

4.1 Introduction

We have introduced system models for both of flat fading channels and frequency-selective fading channels in the previous chapters. In this chapter, we shall analyze the BER of STBC in flat Rayleigh fading channels. Due to the similarity between the decision variables of STBC and Maximum Ratio Combining (MRC), the analysis process is almost the same for them. For the purpose of comparison, the word MRC in this thesis specifically refers to a one transmit, two receive antennas MRC system using BPSK modulation.

Xu [33] analyzed the BER of STBC systems in flat Rayleigh fading channels for BPSK and QPSK with 2 transmit and 1 or 2 receive antennas. The effects of unequal power distribution among 2 transmit antennas were also studied. Vielmon et al [34]

studied the impact of a time-varying flat Rayleigh fading channel on the BER performance of STBC system with 2 transmit and 1 receive antennas and BPSK modulation. BER in the quasi-static channels was derived as a special case of their model.

4.2 BER Analysis in Flat Rayleigh Fading Channels

In the flat Rayleigh fading channels, the fading coefficients between 2 transmit and 1 receive antennas are $h^{(i)}, i = 1,2$. Then the decision metric $\hat{c}_n$ in (2.23) can be further simplified as

$$\begin{aligned}\hat{c}_n &= \sqrt{\frac{E_s}{2}}\left(a_n^{(1)}\left|h^{(1)}\right|^2 + a_n^{(2)}h^{(1)*}h^{(2)} + a_{n+1}^{(1)*}h^{(1)*}h^{(2)} + a_{n+1}^{(2)*}\left|h^{(2)}\right|^2\right) + h^{(1)*}w_n + h^{(2)}w_{n+1}^* \\ &= \sqrt{\frac{E_s}{2}}c_n\left(\left|h^{(1)}\right|^2 + \left|h^{(2)}\right|^2\right) + h^{(1)*}w_n + h^{(2)}w_{n+1}^*\end{aligned} \tag{4.1}$$

where the STBC code mapping as shown in Fig. 2.9 is used to cancel the items $a_n^{(2)}h^{(1)*}h^{(2)}$ and $a_{n+1}^{(1)*}h^{(1)*}h^{(2)}$. Similarly,

$$\hat{c}_{n+1} = \sqrt{\frac{E_s}{2}}c_{n+1}\left(\left|h^{(1)}\right|^2 + \left|h^{(2)}\right|^2\right) + h^{(2)*}w_n - h^{(1)}w_{n+1}^* \tag{4.2}$$

4.2.1 BPSK

For BPSK modulation, without loss of generality, symbol $c_n = 1$ is assumed to be transmitted and all symbols are equally probable. Then, BER is

$$P_e = \Pr\left[\mathrm{Re}\left(\hat{c}_n\right) < 0\right] \tag{4.3}$$

Next, we shall find $\Pr\left[\mathrm{Re}\left(\hat{c}_n\right)<0\right]$ in two steps: firstly, the BER conditioned on the fading gain $h^{(i)}$ is found; secondly, the conditional BER is averaged over the fading statistics. Let $\mathbb{R}_B=\mathrm{Re}\left(\hat{c}_n\right)$, then from (4.1), $h^{(i)}=h_r^{(i)}+jh_i^{(i)}$, $w_n=w_{n,r}+jw_{n,i}$,

$$\mathbb{R}_B=\sqrt{\frac{E_s}{2}}\sum_{i=1}^{2}\left|h^{(i)}\right|^2+h_r^{(1)}w_{n,r}+h_i^{(1)}w_{n,i}+h_r^{(2)}w_{n+1,r}+h_i^{(2)}w_{n+1,i} \tag{4.4}$$

where $E\left[w_{n,r}^2\right]=E\left[w_{n,i}^2\right]=\frac{N_0}{2}$. Conditioning on the fading $h^{(i)}$, $\mathbb{R}_B$ is a Gaussian random variable with

$$E\left[\mathbb{R}_B\mid h^{(i)}\right]=\sqrt{\frac{E_s}{2}}\sum_{i=1}^{2}\left|h^{(i)}\right|^2 \tag{4.5}$$

$$\begin{aligned}E\left[{\mathbb{R}_B}^2\mid h^{(i)}\right]&=E^2\left[\mathbb{R}_B\mid h^{(i)}\right]+E\left[\left(h_r^{(1)}w_{n,r}+h_i^{(1)}w_{n,i}+h_r^{(2)}w_{n+1,r}+h_i^{(2)}w_{n+1,i}\right)^2\right]\\&=E^2\left[\mathbb{R}_B\mid h^{(i)}\right]+\frac{N_0}{2}\sum_{i=1}^{2}\left|h^{(i)}\right|^2\end{aligned} \tag{4.6}$$

Then by looking for the Cumulative Distribution Function of Gaussian random variables, the conditional BER is

$$\begin{aligned}P_e\left(\gamma_b\right)&=\Pr\left[\mathbb{R}_B<0\mid h^{(i)}\right]\\&=\int_{-\infty}^{0}\frac{1}{\sqrt{2\pi\frac{N_0}{2}\sum_{i=1}^{2}\left|h^{(i)}\right|^2}}\exp\left(\frac{-\left(x-\sqrt{\frac{E_s}{2}}\sum_{i=1}^{2}\left|h^{(i)}\right|^2\right)^2}{2\frac{N_0}{2}\sum_{i=1}^{2}\left|h^{(i)}\right|^2}\right)dx\\&=\int_{\sqrt{2\gamma_b}}^{\infty}\frac{1}{\sqrt{2\pi}}\exp\left(\frac{-y^2}{2}\right)dy\\&=Q\left(\sqrt{2\gamma_b}\right)\end{aligned} \tag{4.7}$$

where the instantaneous SNR per bit $\gamma_b=\frac{E_s}{2N_0}\sum_{i=1}^{2}\left|h^{(i)}\right|^2$.

Now, let us derive the statistics of the instantaneous SNR per bit γ_b. Apparently, γ_b is a summation of squares of four independent Gaussian random variables with mean zero and variance $\frac{E_s}{2N_0}\bar{g}_p$, where $E\left[h_r^{(i)2}\right]=E\left[h_i^{(i)2}\right]=\bar{g}_p$. So γ_b has central Chi-square distribution with 4 degrees of freedom with PDF (Chapter 2 of [4]):

$$p_{\gamma_b}(\gamma_b)=\frac{4}{\bar{\gamma}_b^2}\gamma_b\exp\left(\frac{-2\gamma_b}{\bar{\gamma}_b}\right) \tag{4.8}$$

where $E[\gamma_b]=\bar{\gamma}_b=\frac{2E_s}{N_0}\bar{g}_p$.

The final BER can be derived from the integral

$$\begin{aligned}
P_e &= \int_0^\infty P_e(\gamma_b)\,p_{\gamma_b}(\gamma_b)\,d\gamma_b \\
&= \int_0^\infty\left(\int_{\sqrt{2\gamma_b}}^\infty \frac{1}{\sqrt{2\pi}}\exp\left(\frac{-y^2}{2}\right)dy\right)\frac{4}{\bar{\gamma}_b^2}\gamma_b\exp\left(\frac{-2\gamma_b}{\bar{\gamma}_b}\right)d\gamma_b \\
&= \frac{1}{\sqrt{2\pi}}\int_0^\infty\left(\int_{\sqrt{u\bar{\gamma}_b}}^\infty \exp\left(\frac{-y^2}{2}\right)dy\right)u\exp(-u)\,du \\
&= \frac{1}{\sqrt{2\pi}}\int_0^\infty\left(\int_0^{\frac{y^2}{\bar{\gamma}_b}} u\exp(-u)\,du\right)\exp\left(\frac{-y^2}{2}\right)dy
\end{aligned} \tag{4.9}$$

where $u=\frac{2\gamma_b}{\bar{\gamma}_b}$. Since

$$\begin{aligned}
\int_0^{\frac{y^2}{\bar{\gamma}_b}} u\,\mathrm{e}^{-u}\,du &= -\frac{y^2}{\bar{\gamma}_b}e^{-\frac{y^2}{\bar{\gamma}_b}} + \int_0^{\frac{y^2}{\bar{\gamma}_b}}\mathrm{e}^{-u}\,du \\
&= 1-e^{-\frac{y^2}{\bar{\gamma}_b}}-\frac{y^2}{\bar{\gamma}_b}e^{-\frac{y^2}{\bar{\gamma}_b}}
\end{aligned} \tag{4.10}$$

and using the definite integrals

$$\int_0^\infty \mathrm{e}^{-a^2y^2}\,dy=\frac{\sqrt{\pi}}{2a} \tag{4.11}$$

$$\int_0^\infty y^2 \, \mathrm{e}^{-a^2 y^2} \, dy = \frac{\sqrt{\pi}}{4a^3} \tag{4.12}$$

(4.9) can be separated into 3 parts:

$$P_e = I_1 + I_2 + I_3 \tag{4.13}$$

where

$$I_1 = \frac{1}{\sqrt{2\pi}} \int_0^\infty \mathrm{e}^{\frac{-y^2}{2}} \, dy = \frac{1}{2} \tag{4.14}$$

$$I_2 = -\frac{1}{\sqrt{2\pi}} \int_0^\infty \mathrm{e}^{-y^2\left(\frac{1}{2}+\frac{1}{\overline{\gamma}_b}\right)} \, dy = -\frac{1}{2}\sqrt{\frac{\overline{\gamma}_b}{2+\overline{\gamma}_b}} \tag{4.15}$$

$$I_3 = -\frac{1}{\sqrt{2\pi}} \int_0^\infty \frac{y^2}{\overline{\gamma}_b} \mathrm{e}^{-y^2\left(\frac{1}{2}+\frac{1}{\overline{\gamma}_b}\right)} \, dy = -\frac{1}{2}\left(\frac{1}{2+\overline{\gamma}_b}\right)\sqrt{\frac{\overline{\gamma}_b}{2+\overline{\gamma}_b}} \tag{4.16}$$

So the final BER expression is

$$\begin{aligned} P_e &= \frac{1}{2} - \frac{1}{2}\sqrt{\frac{\overline{\gamma}_b}{2+\overline{\gamma}_b}} - \frac{1}{2}\left(\frac{1}{2+\overline{\gamma}_b}\right)\sqrt{\frac{\overline{\gamma}_b}{2+\overline{\gamma}_b}} \\ &= \frac{1}{4}\left(1-\sqrt{\frac{\overline{\gamma}_b}{2+\overline{\gamma}_b}}\right)^2\left(2+\sqrt{\frac{\overline{\gamma}_b}{2+\overline{\gamma}_b}}\right) \end{aligned} \tag{4.17}$$

The above result can also be derived as a specific case of the expression (14.4-15) of [4]. What's more, (14.4-18) of [4] can be utilized as an approximation of (4.17):

$$P_e \approx \frac{3}{4\overline{\gamma}_b^2} \tag{4.18}$$

(4.18) clearly shows BER is proportional to the inverse of the square of averaged SNR per bit, which means STBC achieves the diversity order 2, the full diversity order for a two-branch system.

4.2.2 QPSK

For QPSK modulation, without loss of generality, symbol $\frac{1}{\sqrt{2}}+\frac{j}{\sqrt{2}}$ is assumed to be transmitted and all symbols are equally probable. The decision for the symbol, which has 2 bits, will be wrong if $\hat{c}_n$ falls into the second, third or fourth quadrant. Due to symmetry, The BER is

$$P_{QPSK}=\frac{1}{2}\left(\Pr\left[\hat{c}_n\in Q_2\right]+2\Pr\left[\hat{c}_n\in Q_3\right]+\Pr\left[\hat{c}_n\in Q_4\right]\right) \tag{4.19}$$

where Q_x means the *xth* quadrant. The $\frac{1}{2}$ accounts for the fact each QPSK symbol contains 2 bits. When $\hat{c}_n$ falls into the third quadrant, both bits of the symbol are wrong. So there is a 2 before $\Pr\left[\hat{c}_n\in Q_3\right]$. Since

$$\Pr\left[\hat{c}_n\in Q_2\right]=\Pr\left[\hat{c}_n\in Q_4\right] \tag{4.20}$$

(4.19) can be simplified to

$$\begin{aligned}P_{QPSK}&=\Pr\left[\hat{c}_n\in Q_2\right]+\Pr\left[\hat{c}_n\in Q_3\right]\\&=\Pr\left[\mathrm{Re}\left(\hat{c}_n\right)<0\right]\end{aligned} \tag{4.21}$$

which has the same format with BPSK BER (4.3). Let's $\mathbb{R}_Q=\mathrm{Re}\left(\hat{c}_n\right)$, then

$$\mathbb{R}_Q=\sqrt{\frac{E_s}{4}}\sum_{i=1}^{2}\left|h^{(i)}\right|^2+h_r^{(1)}w_{n,r}+h_i^{(1)}w_{n,i}+h_r^{(2)}w_{n+1,r}+h_i^{(2)}w_{n+1,i} \tag{4.22}$$

Since instantaneous SNR per symbol is $\gamma=\frac{E_s}{2N_0}\sum_{i=1}^{2}\left|h^{(i)}\right|^2$, for QPSK, instantaneous SNR per bit is $\gamma_{Qb}=\frac{E_s}{4N_0}\sum_{i=1}^{2}\left|h^{(i)}\right|^2=\frac{E_b}{2N_0}\sum_{i=1}^{2}\left|h^{(i)}\right|^2$, averaged SNR per bit

$E\left[\gamma_{Qb}\right]=\overline{\gamma}_{Qb}=\frac{E_s}{N_0}\overline{g}_p=\frac{2E_b}{N_0}\overline{g}_p$. If we use E_b and γ_{Qb} instead of E_S and γ, all the variables in QPSK has the same format as that in BPSK. Thus, the final BER is similar to (4.9):

$$P_e=\frac{1}{4}\left(1-\sqrt{\frac{\overline{\gamma}_{Qb}}{2+\overline{\gamma}_{Qb}}}\right)^2\left(2+\sqrt{\frac{\overline{\gamma}_{Qb}}{2+\overline{\gamma}_{Qb}}}\right) \tag{4.23}$$

The conclusion is BPSK and QPSK still have the same performance in flat Rayleigh fading channels.

4.3 BER Results in Flat Rayleigh Fading Channels

In this section, the result for 2 transmit antennas, 1 receive antenna STBC with BPSK in flat Rayleigh fading channels is plotted. Since the analysis is exact, i.e. no approximation is resorted, the result fits well with the simulation in [17].

First, we introduce some BER analysis results for BPSK without transmit diversity as benchmark. The analysis results for BPSK in Gaussian channels is ([4]):

$$P_e=\sqrt{2\gamma_b} \tag{4.24}$$

The analysis results for BPSK in Rayleigh fading channels is ([4]):

$$P_e=\frac{1}{2}\left(1-\sqrt{\frac{\overline{\gamma}_b}{1+\overline{\gamma}_b}}\right) \tag{4.25}$$

The analysis results for BPSK in Rayleigh fading channels with 2 braches MRC is (formula 14.4-15 of [4]):

$$P_e = \frac{1}{4}\left(1-\sqrt{\frac{\overline{\gamma}_{b,MRC}}{2+\overline{\gamma}_{b,MRC}}}\right)^2\left(2+\sqrt{\frac{\overline{\gamma}_{b,MRC}}{2+\overline{\gamma}_{b,MRC}}}\right) \tag{4.26}$$

In (4.26), $\overline{\gamma}_{b,MRC} = E[\gamma_{b,MRC}]$, where the instantaneous SNR $\gamma_{b,MRC} = \frac{E_s}{N_0}\sum_{i=1}^{2}\left|h^{(i)}\right|^2$, E_s is symbol energy, $\frac{N_0}{2}$ is double-sided AWGN power spectrum, $h^{(i)}, i = 1,2$ are fading coefficients between antennas.

Before drawing BER curves, we shall identify a difference in the definition of γ_b in STBC and $\gamma_{b,MRC}$ in MRC. The relation is $\gamma_{b,MRC} = \frac{E_s}{N_0}\sum_{i=1}^{2}\left|h^{(i)}\right|^2 = 2\gamma_b$ and $\overline{\gamma}_{b,MRC} = \frac{4E_s}{N_0}\overline{g}_p = 2\overline{\gamma}_b$. So if the definition of SNR per bit is $\gamma_{b,MRC}$, the BER for STBC in (4.17) should be changed into

$$P_e = \frac{1}{4}\left(1-\sqrt{\frac{\overline{\gamma}_{b,MRC}}{4+\overline{\gamma}_{b,MRC}}}\right)^2\left(2+\sqrt{\frac{\overline{\gamma}_{b,MRC}}{4+\overline{\gamma}_{b,MRC}}}\right) \tag{4.27}$$

This means STBC is 3 dB inferior to MRC if the total transmitted power is the same. We shall use $\gamma_{b,MRC}$ as the definition of SNR per bit for STBC in the following Fig. 4.1.

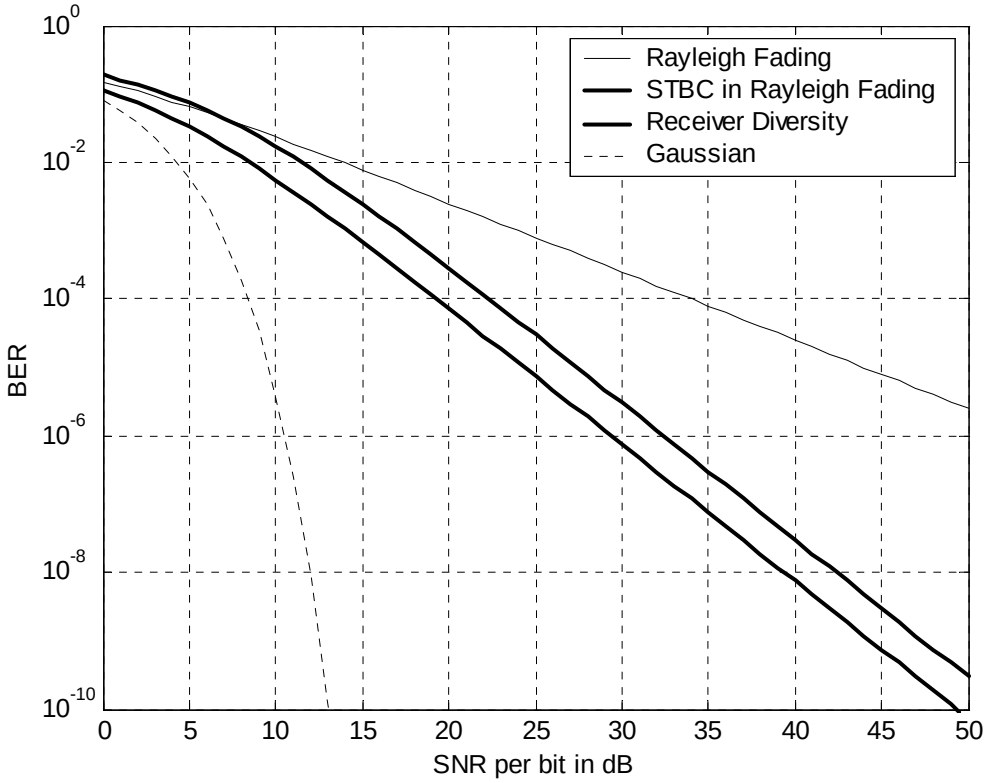

Fig. 4.1 STBC performance in flat Rayleigh fading channel.

Fig. 4.1 shows 3dB performance loss of STBC compared with MRC. The loss results from the fact that the power at each transmit antenna is halved. If the transmitted power on each antenna of STBC is the same as that of MRC, then their performance are identical. Since BER curve of STBC has the same slope as that of MRC, STBC can achieve the full diversity order. Tarokh [18] proves STBC can achieve the full diversity order for general configuration, e.g. using any number of transmit antennas. The performance gain of STBC at a BER of 10^{-4} is 12 dB.

For QPSK in Rayleigh fading channels with 2 braches MRC, the BER expression is still (4.26) (formula 14.4-41 of [4]). That is to say, BPSK and QPSK have the same BER performance in Rayleigh fading channels with 2 braches MRC. BPSK and QPSK still have the same BER performance for STBC in flat Rayleigh fading

channels, as we have shown in (4.17) and (4.23). So the BER curve for QPSK is not separately plotted.

CHAPTER FIVE

Performance Analysis in Frequency-selective Rayleigh Fading Channels

5.1 Introduction

After the BER analysis of STBC in flat Rayleigh fading channels, in this chapter we shall analyze the error rate performance of STBC system in frequency-selective Rayleigh fading channels. The result from this analysis is the main contribution of this thesis.

In a frequency-selective fading channel, bit errors are more likely caused by multipath-induced Inter-symbol Interference (ISI) than by Additive White Gaussian Noise (AWGN). Therefore, in the BER analysis of STBC in frequency-selective fading channels, we ignore the presence of AWGN.

When plotting the BER against SNR, the BER curve settles down to a fixed value as SNR tend to infinity. We call this constant error rate value, the irreducible error

floor, as the Average Irreducible Bit Error Rate (AIBER), which is caused by ISI. When AWGN is ignored, the result from error rate analysis is AIBER.

Our configuration is BPSK, 2 transmit and 1 receive antennas. Signal model in frequency-selective fading channels, first considered in [25] and [26], has been introduced in Chapters 3. The classic general quadratic form [35] is briefly mentioned. The approach to perform AIBER analysis from [27] and [28] is used to find the final AIBER: firstly, the characteristic function (CF) of the decision variable is derived following the steps in appendix B of [4]. Then, conditioning the probability of making a wrong decision on a specific transmitted sequence, we transform the CF into a probability density function (PDF) of the decision variable and then derive the BER expression. Finally, the conditional error probability is averaged over all of the possible sequences to obtain the final BER expression.

5.2 Adaptation of System Model

As we have stated, SNR is set to infinity in the averaged irreducible BER (AIBER) analysis to identify the effects of ISI. So the noise component w_n and signal energy E_s are dropped from our previously introduced signal model for convenience.

Substituting r_n and r_{n+1} of (3.21) into (3.26):

$$\hat{c}_n = \sum_{m=-1}^{1} a_{n-m}^{(1)} d_m^{(1)} d_0^{(1)*} + \sum_{m=-1}^{1} a_{n-m}^{(2)} d_m^{(2)} d_0^{(1)*} + \sum_{m=-1}^{1} a_{n-m+1}^{(1)*} d_m^{(1)*} d_0^{(2)} + \sum_{m=-1}^{1} a_{n-m+1}^{(2)*} d_m^{(2)*} d_0^{(2)} \tag{5.1}$$

When $m=0$, we can cancel the items containing c_{n+1}, which are $a_n^{(2)}d_0^{(2)}d_0^{(1)*}$ and $a_{n+1}^{(1)*}d_0^{(1)*}d_0^{(2)}$ in (5.1), due to the structure of STBC. Thus we have

$$\begin{aligned}\hat{c}_n = &\sum_{m=-1}^{1} a_{n-m}^{(1)}d_m^{(1)}d_0^{(1)*} + \sum_{m=-1,1} a_{n-m}^{(2)}d_m^{(2)}d_0^{(1)*} \\ &+ \sum_{m=-1,1} a_{n-m+1}^{(1)*}d_m^{(1)*}d_0^{(2)} + \sum_{m=-1}^{1} a_{n-m+1}^{(2)*}d_m^{(2)*}d_0^{(2)}\end{aligned} \tag{5.2}$$

The AIBER conditioned on a specific transmitted sequence Γ_p is equal to the probability to make a wrong decision for $\hat{c}_n$. Without loss of generality, let $c_n=1$. The conditional error probability on Γ_p is equal to

$$P_{e|\Gamma_p} = \Pr\left[\mathrm{Re}\left(\hat{c}_n\right)<0\right] \tag{5.3}$$

5.3 General Quadratic Form

In order to evaluate (5.3), we shall first review the classic work on the general quadratic form ([35], appendix B of [4]). The decision variable of a multichannel receiver for binary signal can be written in the general quadratic form

$$D=\sum_{l=1}^{L}[A|X_l|^2 + B|Y_l|^2 + CX_l^*Y_l + C^*X_lY_l^*] \tag{5.4}$$

where *A*, *B*, and *C* are constants, X_l and Y_l are a pair of correlated complex Gaussian random variables and different pairs of $\{X_l, Y_l\}$ are mutually independent and identically distributed (iid). L is the order of diversity. Thus for example, in the case of incoherent detection, *A*=1, *B*=-1, and *C*=0, while for coherent detection, *A*=*B*=0 and *C*=1. The error probability is found by comparing *D* with zero in a zero threshold

device whose output is "1" say, if the threshold is exceeded and "0" if the threshold is not exceeded.

Bello [35] provides a solution for $\Pr[D<0]$. Proakis [4] presents an alternative way to get $\Pr[D<0]$. A derivation similar to [4] is used here.

We can observe the similarity between our decision variable and the general quadratic form. If we can define

$$\begin{cases} X_1 = \sum_{m=-1}^{1} a_{n-m}^{(1)} d_m^{(1)} + \sum_{m=-1,1} a_{n-m}^{(2)} d_m^{(2)} \\ Y_1 = d_0^{(1)} \\ X_2 = \sum_{m=-1,1} a_{n-m+1}^{(1)*} d_m^{(1)*} + \sum_{m=-1}^{1} a_{n-m+1}^{(2)*} d_m^{(2)*} \\ Y_2 = d_0^{(2)*} \end{cases} \tag{5.5}$$

Then

$$\begin{aligned} P_{e|\Gamma_p} &= \Pr\left[\mathrm{Re}\left(\hat{c}_n\right)<0\right] \\ &= \Pr[\sum_{l=1,2}\left(X_l^* Y_l + X_l Y_l^*\right)<0] \end{aligned} \tag{5.6}$$

where we used the relation $\Pr\left[\mathrm{Re}\left(z\right)<0\right]=\Pr\left[\left(z+z^*\right)/2<0\right]=\Pr\left[\left(z+z^*\right)<0\right]$, z can be any complex number.

However, in our case, different pairs of $\{X_l, Y_l\}$ are neither identically distributed nor mutually independent since X_1 and X_2 are conditioned on different sequences and have common factors in their expressions. The shadowed areas in Fig. 5.1 and Fig. 5.2 show the symbols on which X_1 and X_2 are conditioned.

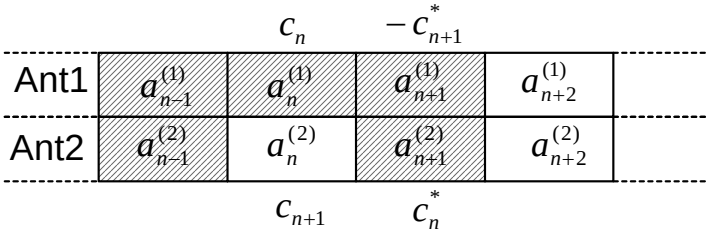

Fig. 5.1 The symbols on which X_1 is conditioned.

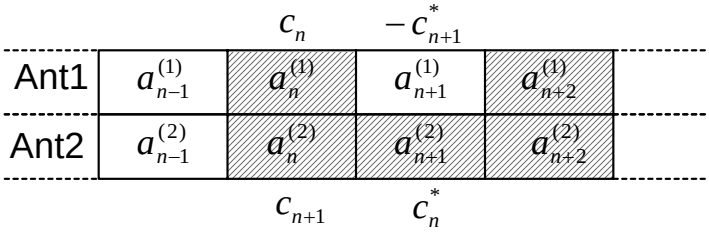

Fig. 5.2 The symbols on which X_2 is conditioned.

If the RMS delay spread is small, $d_0^{(i)} >> d_m^{(i)}$ for $m \neq 0$. This means that the cross-correlations between different pairs of $\{X_l, Y_l\}$ are small and we can approximate it as independent. Numerical results in Chapter 6 give examples of the cross-correlations and verified the appropriateness of the approximation. Another problem is different pairs of $\{X_l, Y_l\}$ have different distribution. Hence, to solve (5.6), we have to proceed step by step instead of directly using the results in [4].

5.4 AIBER Analysis

Following the steps in [4] and noting in our case, $A = B = 0, C = 1$, $\overline{X}_l = \overline{Y}_l = 0$, the characteristic function of $\hat{c}_n$ is simplified into

$$\psi_{\hat{c}_n}(jv) = \prod_{k=1,2} \frac{v_{k1} v_{k2}}{(v + jv_{k1})(v - jv_{k2})} \tag{5.7}$$

where

$$\begin{cases} v_{k1} = \sqrt{w_k^2 + (1/4)(\mu_{kxx}\mu_{kyy} - |\mu_{kxy}|^2)^{-1}} - w_k \\ v_{k2} = \sqrt{w_k^2 + (1/4)(\mu_{kxx}\mu_{kyy} - |\mu_{kxy}|^2)^{-1}} + w_k \\ w_k = \dfrac{\mu_{kxy}^* + \mu_{kxy}}{4\left(\mu_{kxx}\mu_{kyy} - |\mu_{kxy}|^2\right)} \\ \mu_{kxy} = \dfrac{1}{2}E\left[X_k Y_k^*\right] \end{cases} \tag{5.8}$$

The second order statistics μ_{1xx} is

$$\begin{aligned} \mu_{1xx} &= \frac{1}{2}E\left[\left(\sum_{m=-1}^{1} a_{n-m}^{(1)} d_m^{(1)} + \sum_{m=-1,1} a_{n-m}^{(2)} d_m^{(2)}\right)\left(\sum_{k=-1}^{1} a_{n-k}^{(1)} d_k^{(1)} + \sum_{k=-1,1} a_{n-k}^{(2)} d_k^{(2)}\right)^*\right] \\ &= \sum_{m=-1}^{1}\sum_{k=-1}^{1} a_{n-m}^{(1)} a_{n-k}^{(1)*} d_{m,k} + \sum_{m=-1,1}\sum_{k=-1,1} a_{n-m}^{(2)} a_{n-k}^{(2)*} d_{m,k} \end{aligned} \tag{5.9}$$

in which

$$d_{m,k} = \int_{-\infty}^{\infty} p(mT-\tau)\, p^*(kT-\tau) R_h(\tau) d\tau \tag{5.10}$$

Note that $d_{m,k}$ is the autocorrelation of $d_m^{(i)}$ defined in (3.19). Since the fading is independent and has the same statistics for different transmit antennas, the autocorrelation of $d_m^{(i)}$ is equal to zero if *i* is different in $E\left[d_m^{(i)} d_k^{(i)}\right]$. So we can drop *i* in $d_{m,k}$. Similarly,

$$\mu_{2xx} = \sum_{m=-1,1}\sum_{k=-1,1} a_{n-m+1}^{(1)} a_{n-k+1}^{(1)*} d_{m,k} + \sum_{m=-1}^{1}\sum_{k=-1}^{1} a_{n-m+1}^{(2)} a_{n-k+1}^{(2)*} d_{m,k} \tag{5.11}$$

$$\mu_{1yy} = \mu_{2yy} = d_{0,0}\,, \tag{5.12}$$

$$\begin{aligned} \mu_{1xy} &= \frac{1}{2}E\left[\left(\sum_{m=-1}^{1} a_{n-m}^{(1)} d_m^{(1)} + \sum_{m=-1,1} a_{n-m}^{(2)} d_m^{(2)}\right) d_0^{(1)*}\right] \\ &= \sum_{m=-1}^{1} a_{n-m}^{(1)} d_{m,0} \end{aligned} \tag{5.13}$$

$$\begin{aligned}\mu_{2xy} &= \frac{1}{2}E\left[\left(\sum_{m=-1,1} a_{n-m+1}^{(1)*} d_m^{(1)*} + \sum_{m=-1}^{1} a_{n-m+1}^{(2)*} d_m^{(2)*}\right) d_0^{(2)}\right] \\ &= \sum_{m=-1}^{1} a_{n-m+1}^{(2)*} d_{m,0}\end{aligned} \tag{5.14}$$

Apparently, the second order statistics of X_1 and X_2 are different since they are conditioned on different symbols. The variances μ_{kxx} and μ_{kyy} are always positive and $\mu_{kxx}\mu_{kyy} > \left|\mu_{kxy}\right|^2$ (According to the properties of random variables, the correlation coefficient is always not greater than 1). Another important observation is that μ_{kxx}, μ_{kyy}, μ_{kxy}, v_{k1} and v_{k2} are real since BPSK symbols, pulse shapes and PDP are all real. Then we can conclude $v_{k1} > 0$ and $v_{k2} > 0$. This conclusion will be used in the evaluation of (5.15) to determine the positions of residuals, which is crucial to find the correct results of integrals. Numerical results in Chapter 6 give examples of the second order statistics and $d_{m,k}$.

Using B-4 in [4], the error probability conditioned on a specific transmitted sequence Γ_p is

$$\begin{aligned}P_{e|\Gamma_p} &= \Pr\left[\mathrm{Re}\left(\hat{c}_n\right) < 0\right] = -\frac{1}{2\pi j}\int_{-\infty+j\varepsilon}^{\infty+j\varepsilon} \frac{\psi_{\hat{c}_n}(jv)}{v} dv \\ &= -\frac{1}{2\pi j}\int_{-\infty+j\varepsilon}^{\infty+j\varepsilon} \frac{v_{11}v_{12}v_{21}v_{22}}{v\left(v+jv_{11}\right)\left(v+jv_{21}\right)\left(v-jv_{12}\right)\left(v-jv_{22}\right)} dv\end{aligned} \tag{5.15}$$

To evaluate this integral, two complex integrals are introduced (Appendix A provides proof):

$$\int_{-\infty+j\varepsilon}^{\infty+j\varepsilon} \frac{dv}{v+jv_{k1}} = -\pi\, j \tag{5.16}$$

$$\int_{-\infty+j\varepsilon}^{\infty+j\varepsilon} \frac{dv}{v-jv_{k2}} = \pi\, j \tag{5.17}$$

Both v_{k1} and v_{k2} are real positive numbers as we have previously pointed out. In (5.16), the pole is below the integral path while it's above the path in (5.17). Then (5.15) can be further developed as

$$\begin{aligned} P_{e|\Gamma_p} &= -\frac{1}{2\pi j}\int_{-\infty+j\varepsilon}^{\infty+j\varepsilon} \frac{v_{11}v_{12}v_{21}v_{22}}{v\left(v+jv_{11}\right)\left(v+jv_{21}\right)\left(v-jv_{12}\right)\left(v-jv_{22}\right)}dv \\ &= -\frac{1}{2\pi j}\int_{-\infty+j\varepsilon}^{\infty+j\varepsilon}\left(\frac{1}{v}+\frac{M}{v+jv_{11}}+\frac{N}{v+jv_{21}}+\frac{O}{v-jv_{12}}+\frac{P}{v-jv_{22}}\right)dv \\ &= \frac{v_{11}v_{21}\left(v_{12}^2+v_{12}\left(v_{21}+v_{22}\right)+v_{22}\left(v_{21}+v_{22}\right)+v_{11}\left(v_{12}+v_{21}+v_{22}\right)\right)}{\left(v_{11}+v_{12}\right)\left(v_{12}+v_{21}\right)\left(v_{11}+v_{22}\right)\left(v_{21}+v_{22}\right)} \end{aligned} \tag{5.18}$$

where

$$M = \frac{v_{12}v_{21}v_{22}}{\left(v_{11}+v_{12}\right)\left(v_{11}-v_{21}\right)\left(v_{11}+v_{22}\right)}$$

$$N = \frac{-v_{11}v_{12}v_{22}}{\left(v_{11}-v_{21}\right)\left(v_{12}+v_{21}\right)\left(v_{21}+v_{22}\right)}$$

$$O = \frac{v_{11}v_{21}v_{22}}{\left(v_{11}+v_{12}\right)\left(v_{12}+v_{21}\right)\left(v_{12}-v_{22}\right)}$$

$$P = \frac{-v_{11}v_{12}v_{21}}{\left(v_{12}-v_{22}\right)\left(v_{11}+v_{22}\right)\left(v_{21}+v_{22}\right)}$$

If $v_{11}=v_{21}=v_1$, $v_{12}=v_{22}=v_2$, which means different pairs of $\{X_l, Y_l\}$ in (5.4) are identically distributed, then

$$P_{e|\Gamma_p} = \frac{1+3\dfrac{v_2}{v_1}}{\left(1+\dfrac{v_2}{v_1}\right)^3} \tag{5.19}$$

This agrees with the results in [4].

With $P_{e|\Gamma_p}$ in hand, we can develop P_e by averaging $P_{e|\Gamma_p}$ over all possible Γ_p. The undetermined symbols are $a_{n-1}^{(1)}$, $a_{n+2}^{(1)}$, $a_{n-1}^{(2)}$, $a_{n+2}^{(2)}$ and c_{n+1}. Therefore, there are 32 possible sequences for Γ_p. The final AIBER expression is

$$P_e = \frac{1}{32}\sum_{p=1}^{32} P_{e|\Gamma_p} \tag{5.20}$$

CHAPTER SIX

Numerical Results

6.1 Introduction

The analyses results in Chapter 5 are computed here. Some intermediate variables are plotted to demonstrate their properties.

6.2 Properties of the Second Order Statistics

Here we study the properties of the second order statistics of $\{X_l, Y_l\}$. Since the final AIBER is composed of the second order statistics of $\{X_l, Y_l\}$, the impacts of RMS delay spread and PDP on the second order statistics have close relation with AIBER.

First, we study the important term in the second order statistics (5.10):

$$d_{m,k} = \int_{-\infty}^{\infty} p(mT-\tau)\, p^*(kT-\tau) R_h(\tau) d\tau \tag{6.1}$$

where $p(t)$ is the combined pulse shape at transmitter and receiver, $R_h(\tau)$ is power delay profile. The shapes of $d_{m,k}$ are very helpful to explain the shapes of the second

order statistics. For double-spike PDP it is easy to see $d_{m,k} = d_{-m,-k}$. So we confine our choice of m,k within positive values. Using rectangular pulse, $d_{m,k}$ is plotted against the normalized RMS delay spread *d* with different pairs of m,k in Fig. 6.1.

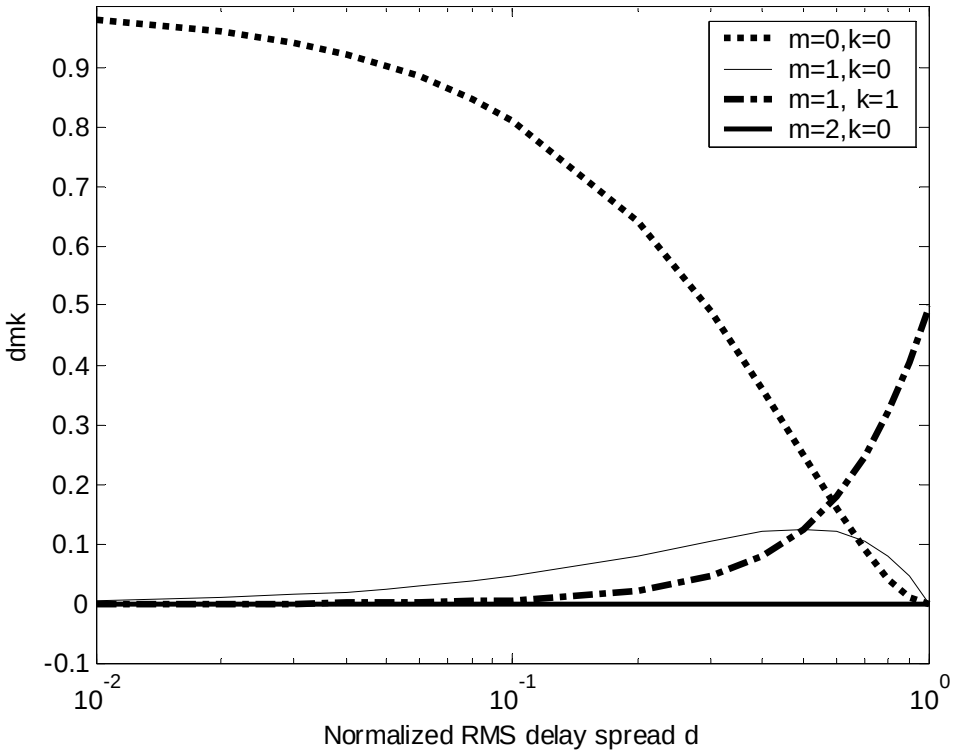

Fig. 6.1 $d_{m,k}$ for double-spike PDP and rectangular pulse.

$d_{0,0}$ is the desired response for current symbol while $d_{m,k}$ with other values of *m* and *k* are interference contributed from adjacent symbols. The ratio $\frac{d_{0,0}}{d_{m,k}}, m \neq 0, k \neq 0$ is the index indicating the severeness of interferences. In flat fading channels, $d_{0,0} = 1$ and $d_{m,k} = 0$ *for* $m \neq 0$ *or* $k \neq 0$. When RMS delay spread $d < 0.1$, Fig. 6.1 shows $d_{0,0} > 0.8$ and $d_{m,k} < 0.1$ *for* $m \neq 0$ *or* $k \neq 0$, which means the signal quality is good. On the other hand, when RMS delay spread $d > 0.5$, the desired component $d_{0,0}$ is

less than the sum of interferences, which means the signal quality is poor and some signal processing techniques, such as equalization, should be adopted.

The bold line at the bottom indicates $d_{m,k} \approx 0$ *for* $m = 2, k = 0$. We can also verify $d_{m,k} \approx 0$ *for* $m = 2, k = 1$ and $d_{m,k} \approx 0$ *for* $m = 2, k = 2$. This corroborates our assumption that the restriction on m, k within $[-1,1]$ will not affect accuracy.

When raised cosine pulse shapes with roll-off factor $\alpha = 0.2$ and $\alpha = 0.8$ are used, $d_{m,k}$ increases a little as Fig. 6.2 displays. For example, at $d = 0.1$, $d_{0,0}$ is increased from about 0.8 in rectangular pulse to about 0.95 in RC pulse. The increase for RC pulse with $\alpha = 0.2$ is little more than that for RC pulse with $\alpha = 0.8$. All of the curves in Fig. 6.1 and Fig. 6.2 keep the same relative positions and $d_{2,0}$ remains very close to 0.

Fig. 6.3 shows $d_{m,k}$ for Gaussian PDP and exponential PDP. Raised cosine pulse shape with roll-off factor $\alpha = 0.8$ is used for both of the two PDP. The impact of PDP on $d_{m,k}$ is much more obvious that that of pulse shape. Since the shape of exponential PDP is asymmetrical, $d_{m,k} \neq d_{-m,-k}$ as we can see from the Fig. 6.3 (b).

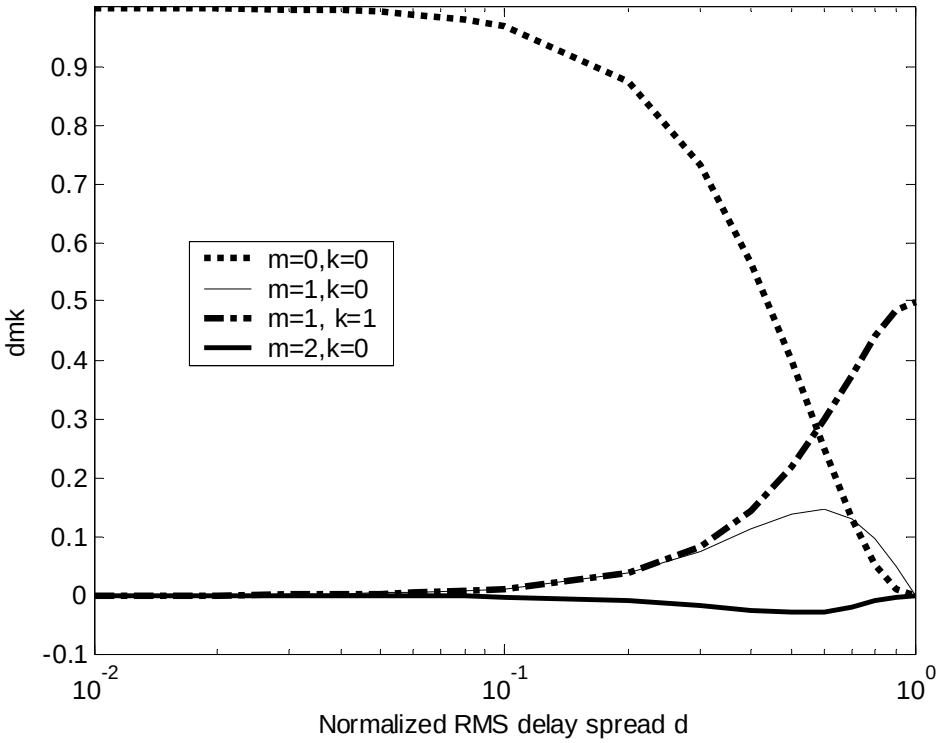

(a)

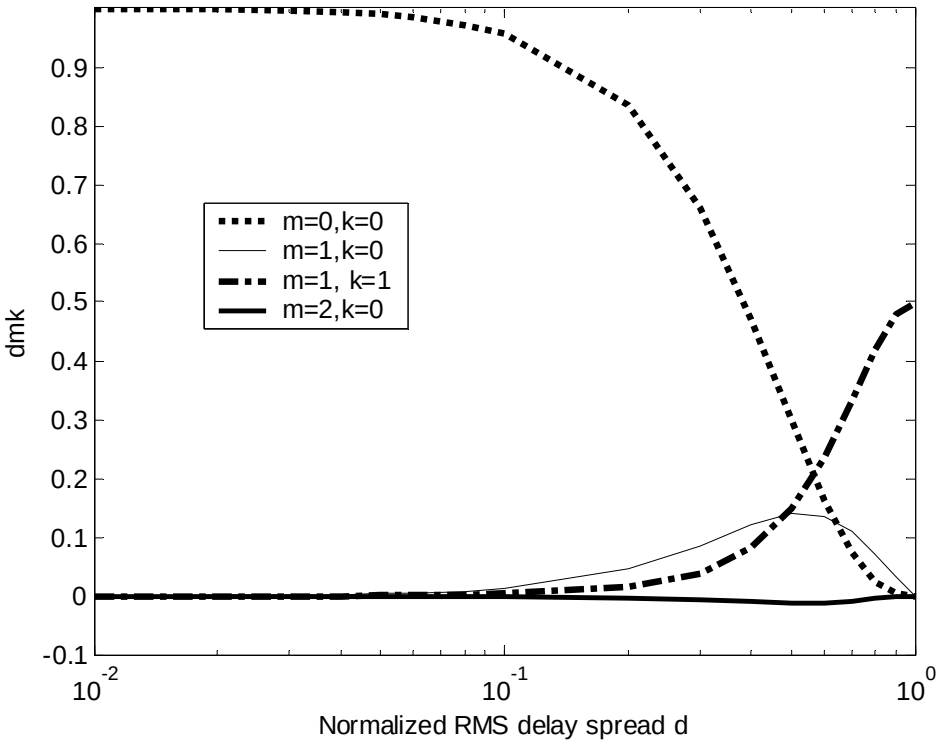

(b)

Fig. 6.2 $d_{m,k}$ **for double-spike PDP and RC pulse with (a)** $\alpha = 0.2$**, (b)** $\alpha = 0.8$**.**

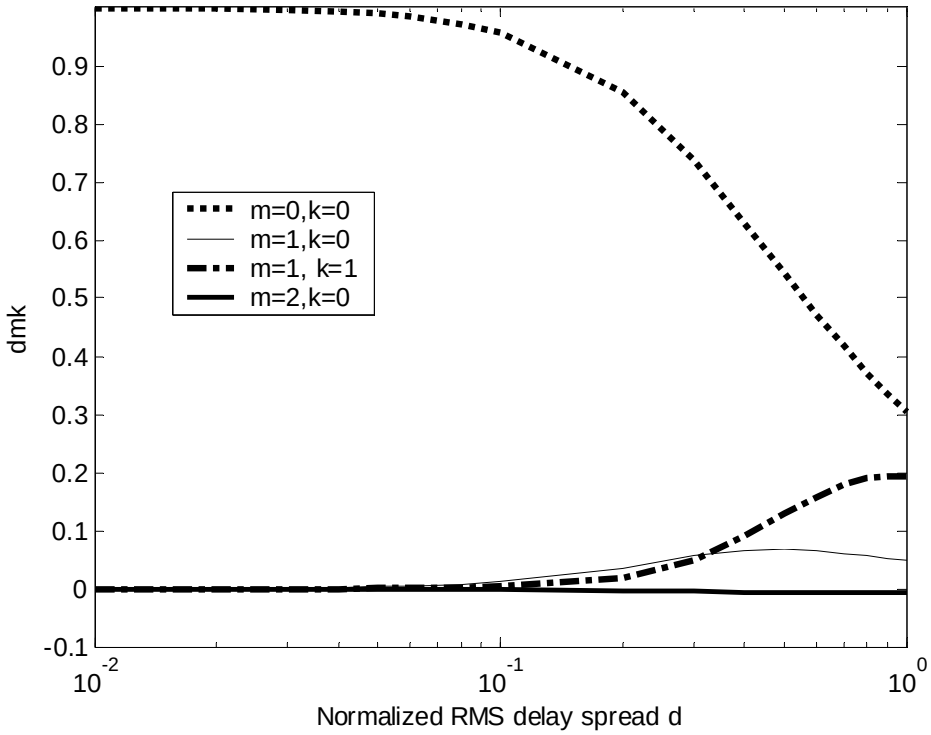

(a)

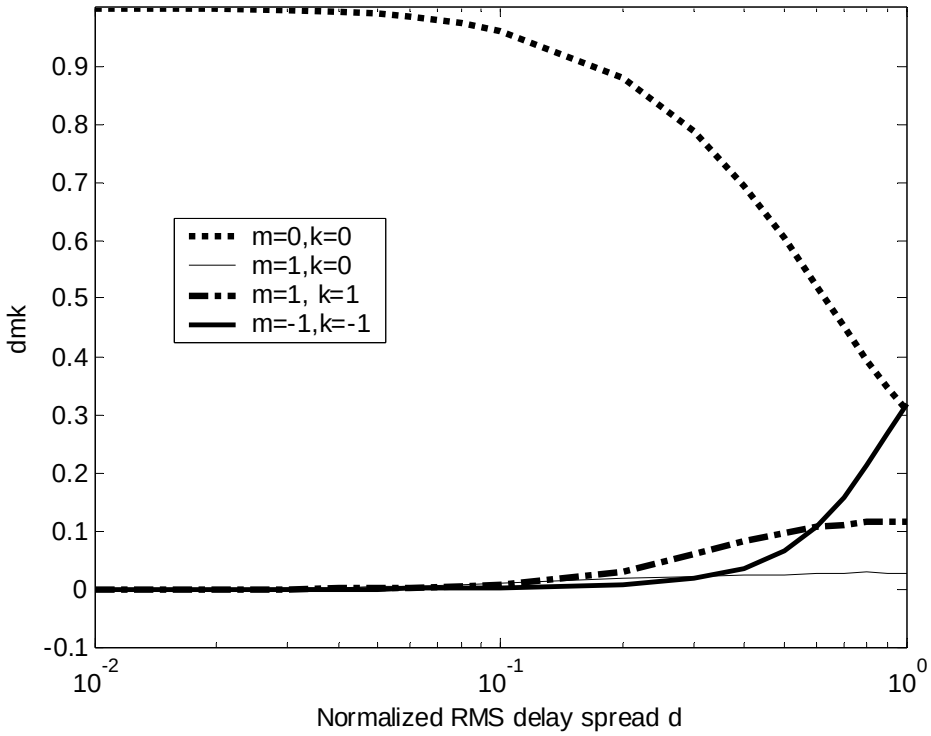

(b)

Fig. 6.3 $d_{m,k}$ for (a) Gaussian PDP, (b) exponential PDP and RC pulse.

Now, we move to the second order statistics of $\{X_l, Y_l\}$:

$$\mu_{1xx} = \sum_{m=-1}^{1}\sum_{k=-1}^{1} a_{n-m}^{(1)} a_{n-k}^{(1)*} d_{m,k} + \sum_{m=-1,1}\sum_{k=-1,1} a_{n-m}^{(2)} a_{n-k}^{(2)*} d_{m,k} \tag{6.2}$$

which is the variance of X_1,

$$\mu_{1xy} = \sum_{m=-1}^{1} a_{n-m}^{(1)} d_{m,0} \tag{6.3}$$

which is the covariance between X_1 and Y_1.

To verify our assumption that the cross-correlations between different pairs of $\{X_l, Y_l\}$ are small, we derive the covariance between X_2 and Y_1 as an example:

$$\begin{aligned} \mu_{x2y1} &= \frac{1}{2} E\left[\left(\sum_{m=-1,1} a_{n-m+1}^{(1)*} d_m^{(1)*} + \sum_{m=-1}^{1} a_{n-m+1}^{(2)*} d_m^{(2)*}\right) d_0^{(1)*}\right] \\ &= \sum_{m=-1,1} a_{n-m+1}^{(1)} d_{m,0} \end{aligned} \tag{6.4}$$

These second order statistics are conditioned on a specific transmitted sequence. As we point out in the previous chapter, there are 32 possible sequences and the final statistics must be averaged over all of the possible sequences. $\bar{\mu}_{1xx}$, $\bar{\mu}_{1xy}$ and $\bar{\mu}_{x2y1}$ are used to denote the averaged statistics. Fig. 6.4 shows the three averaged statistics versus normalized RMS delay spread using double-spike PDP and rectangular pulse.

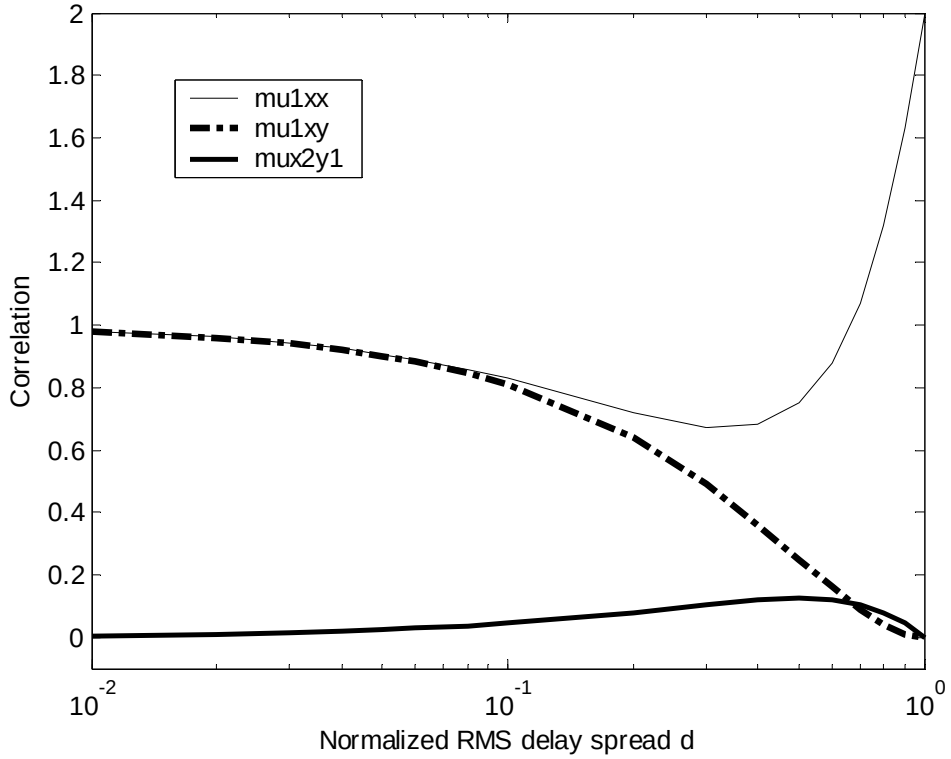

Fig. 6.4 The statistics for double-spike PDP and rectangular pulse.

The curve of $\bar{\mu}_{x2y1}$ verified our approximation that the cross-correlations between different pairs of $\{X_l, Y_l\}$ are small. Its maximum is about 0.12 when $d = 0.5$. The shape of the curve is closely related to that of $d_{1,0}$ since we have assumed $a_n^{(1)} = 1$, but $a_{n+2}^{(1)}$ is random and will not contribute anything to $\bar{\mu}_{x2y1}$.

$d_{0,0}$ and $a_n^{(1)}$ is the deterministic part of $\bar{\mu}_{1xy}$. As $d_{0,0}$ decreased to 0, $\bar{\mu}_{1xy}$ too.

The behavior of $\bar{\mu}_{1xx}$ is interesting since it increases to 2 at $d = 1$. The reason is $\bar{\mu}_{1xx}$ contain the multiplication $a_{n-m}^{(1)} a_{n-k}^{(1)*}$. When *m*=*k*, the multiplication results in a fixed 1, which makes all terms containing $d_{0,0}$, $d_{1,1}$, $d_{-1,-1}$ will contribute to $\bar{\mu}_{1xx}$. At the beginning $d = 0$, $d_{1,1}$ and $d_{-1,-1}$ are 0 and $d_{0,0} = 1$. Thus the correlation is 1. Then variance (we use the term correlation on *y* axis of the figures) decreases as $d_{0,0}$

decreases, while $d_{1,1}$ and $d_{-1,-1}$ remain small. But when the RMS delay spread increases to 1, $d_{1,1}$ and $d_{-1,-1}$ increase to 0.5 and $d_{0,0} = 0$. There are four terms containing $d_{1,1}$ or $d_{-1,-1}$, so the result is 2.

Due to the close relation between the statistics and $d_{m,k}$, pulse shapes do affect the statistics a little since they affect $d_{m,k}$ a little. Between the 2 graphs in Fig. 6.5, the curves of the one using $\alpha = 0.8$ RC pulse are more alike to that using rectangular pulse.

Fig. 6.6 shows the three averaged statistics versus normalized RMS delay spread using Gaussian PDP and exponential PDP. RC pulse with roll-off factor 0.8 is assumed. Similar to $d_{m,k}$, the effects of PDP are more obvious than that of pulse shapes.

Although the relationship between the statistics and $d_{m,k}$ is easy to find, the relationship between the statistics and AIBER is much more complex as (5.20) shows. However, a qualitative prediction is still possible at some points. At small RMS delay spread, all PDP and pulse shapes should have similar AIBER performance since the statistics are very close. When RMS delay spread is large, the prediction is difficult.

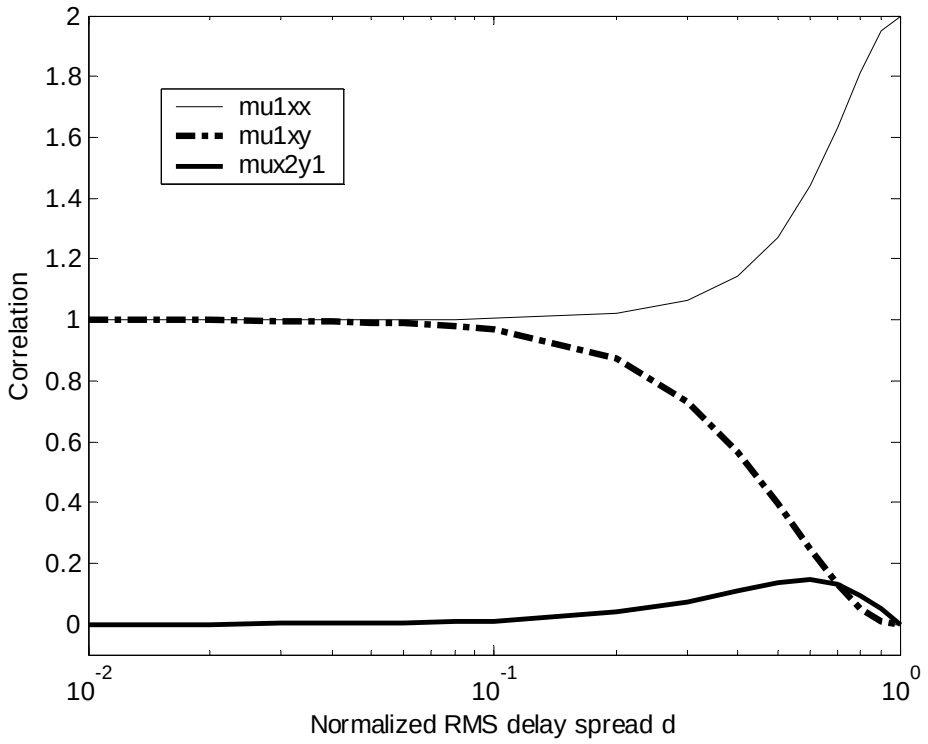

(a)

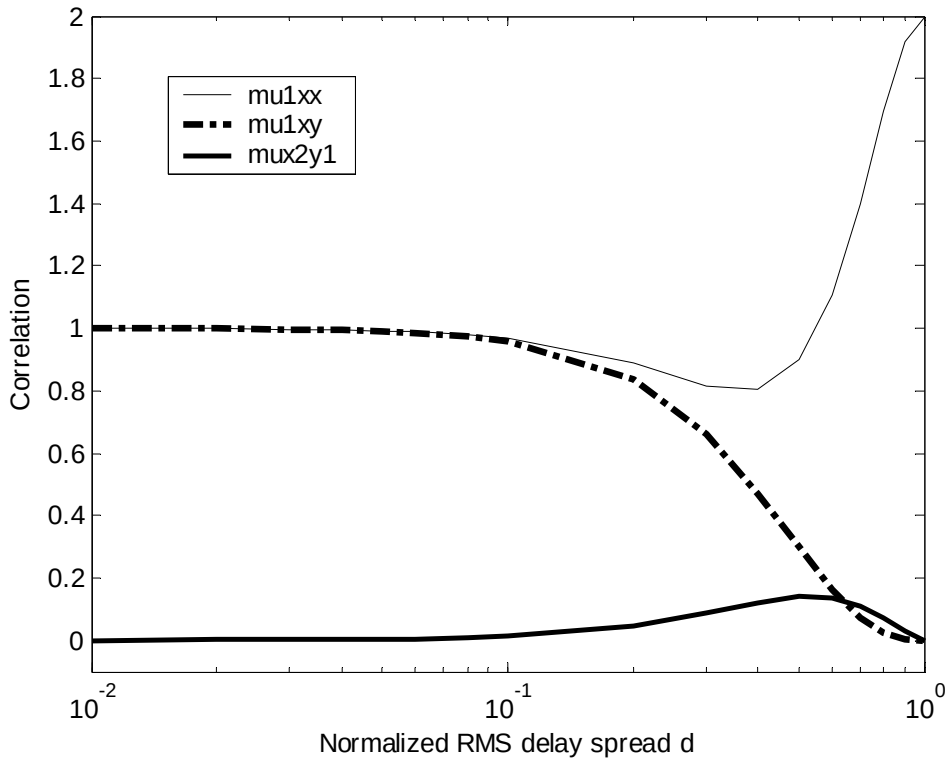

(b)

Fig. 6.5 The statistics for double-spike PDP and RC pulse with (a) $\alpha = 0.2$ **, (b)** $\alpha = 0.8$ **.**

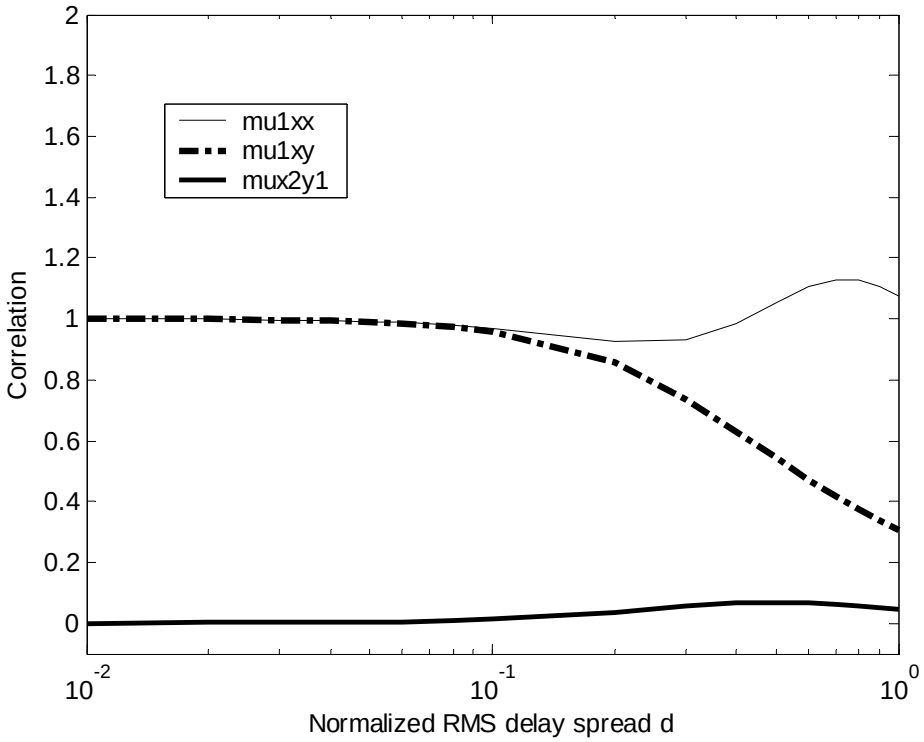

(a)

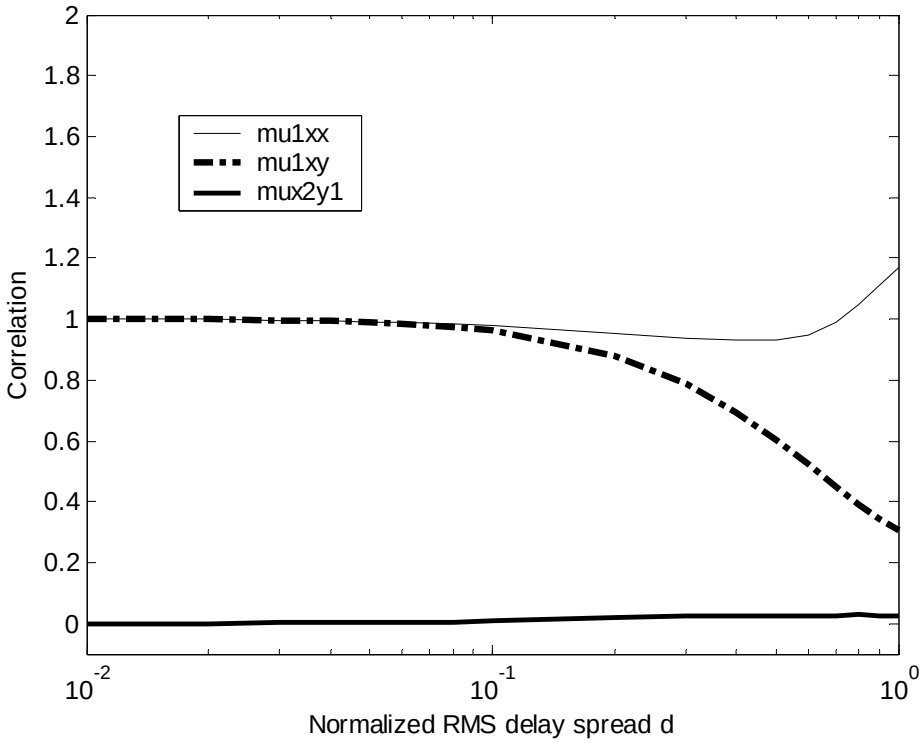

(b)

Fig. 6.6 The statistics for (a) Gaussian PDP and (b) exponential PDP.

6.3 AIBER in Frequency-selective Rayleigh Fading Channels

To get numerical results for (5.20), PDP and pulse function should be specified. As we have mentioned, the sampling time is locked to τ_{mean}, which is set to 0.

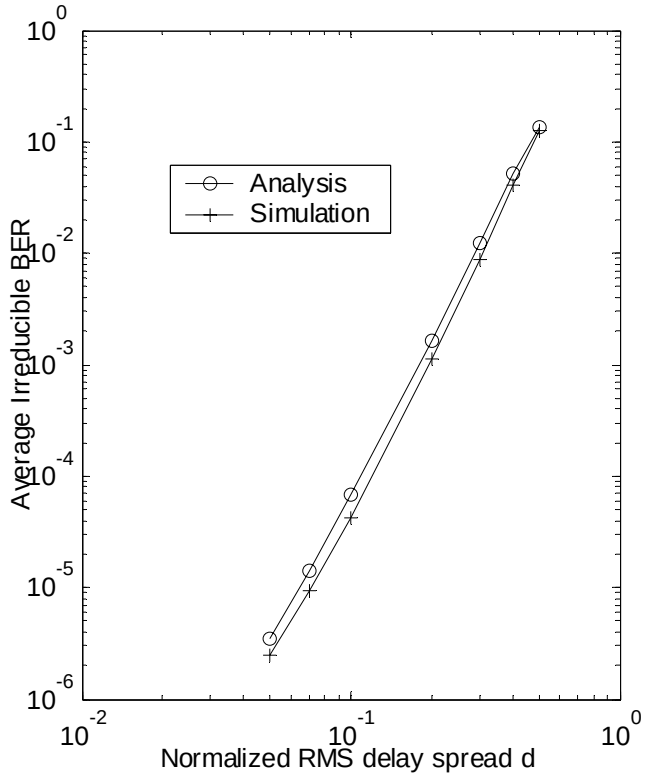

Fig. 6.7 Results of analysis and simulation with rectangular pulse.

In Fig. 6.7, the analysis results are compared with simulation results for STBC in frequency-selective Rayleigh fading channels with double-spike PDP and rectangular pulse. The system model in Fig. 2.8 is used. Since PDP is double-spike, the expression in (3.24) and (3.25) can be utilized to avoid oversampling. The analysis results are very close to simulation results.

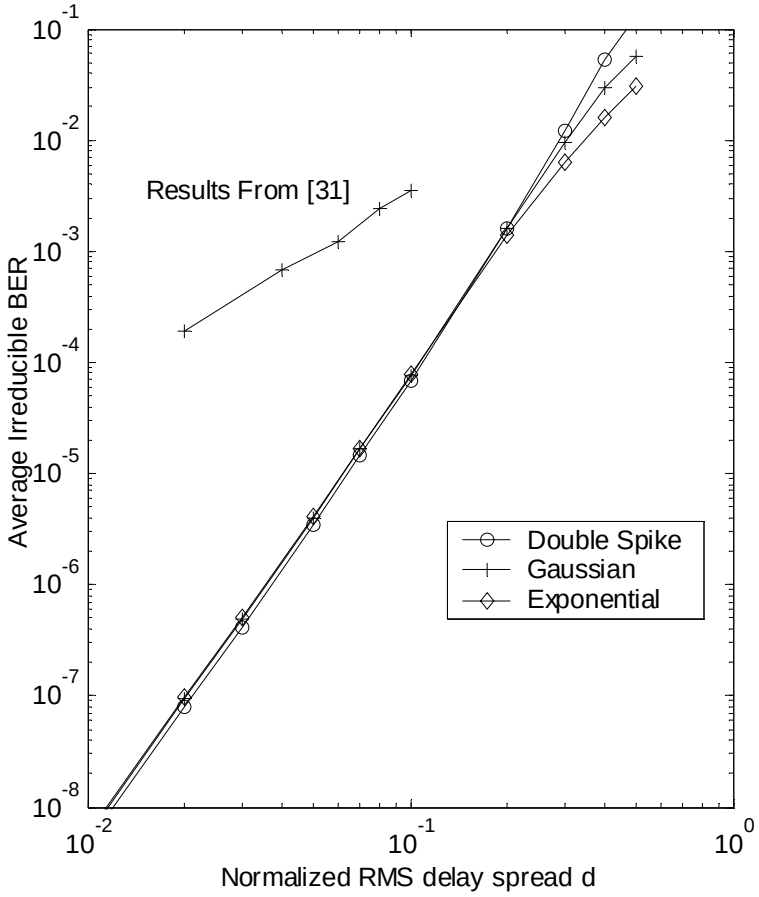

Fig. 6.8 AIBER of different PDP with rectangular pulse.

Fig. 6.8 shows AIBER versus normalized RMS delay spread *d* for 3 kinds of PDP using rectangular pulse. The AIBER from simulation for BPSK without transmit diversity in frequency-selective Rayleigh fading channels with Gaussian PDP [31] is included for comparison. The shape of PDP has little effects on AIBER as long as $d < 0.2$. With a close look, we can find the performance of double-spike PDP is a little bit better then the others. This is because when *d* is small, signal energy of double-spike PDP is concentrated at the sampling point and the ISI effect is not obvious, while the tail of other PDP generate ISI. The situation is reversed when $d > 0.2$: both peaks of double-spike PDP are far from sampling time and both of them generate severe ISI, while sampling time is on the peak of Gaussian PDP and near the peak of one-sided exponential PDP.

An important observation from Fig. 6.8 is that a power-of-four dependence on the RMS delay spread for AIBER is found, while the relation is power-of-two in plain BPSK system [31]. The AIBER is significantly lowered compared with plain BPSK. The implication is that STBC achieves full diversity order and is a powerful tool to combat frequency-selective fading.

In Fig. 6.9, Fig. 6.10 and Fig. 6.11, we show AIBER versus the α of raised-cosine pulse shaping function for 3 kinds of PDP. 3 RMS delay spread values are chosen: 0.05, 0.2 and 0.4. At the right side of the figures, the discrete points show the AIBER of rectangular pulse with the same RMS delay spread for each kind of the PDP.

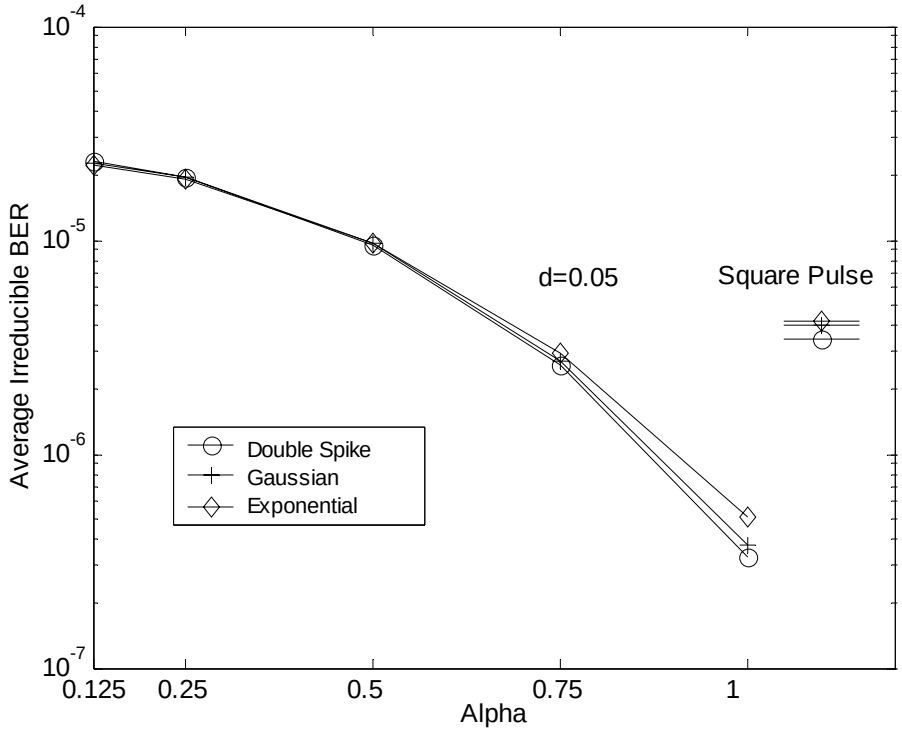

Fig. 6.9 AIBER versus α of RC filter for different PDP and d=0.05.

When *d=0.05*, the performance is the same for all PDP if $\alpha < 0.75$. After this point, exponential PDP is inferior to the others.

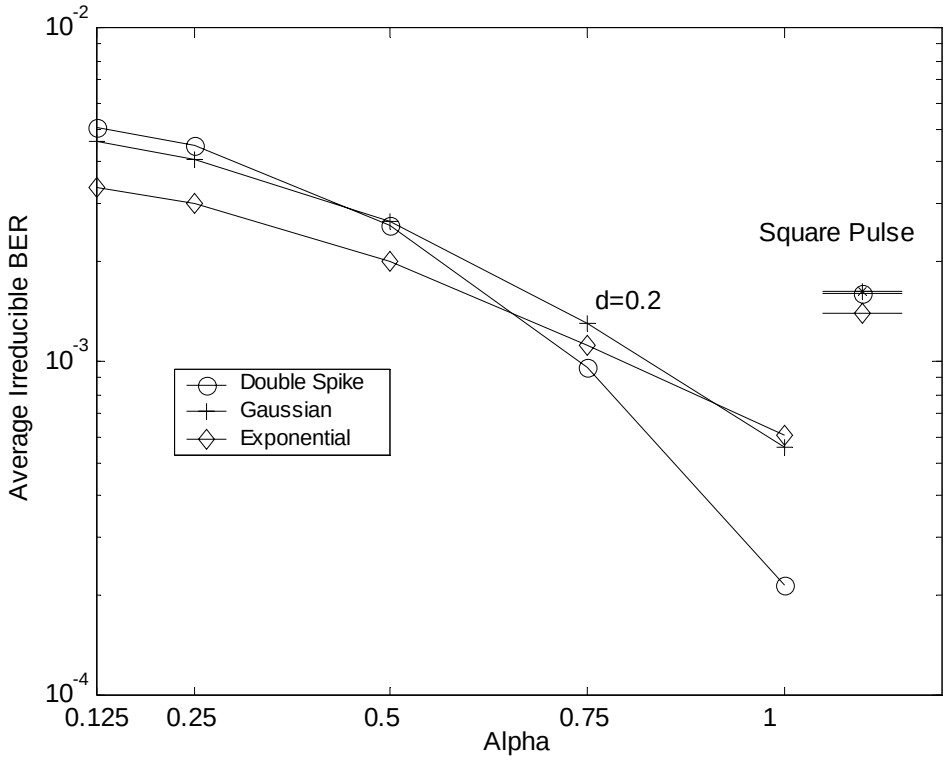

Fig. 6.10 AIBER versus α of RC filter for different PDP and d=0.2.

When *d=0.2*, the three curves are mingled for a while. If the bandwidth is wide (α is close to 1), double-spike PDP is superior to the others. At the other side of the curves, the performance of double-spike PDP is degraded by ISI due to limited bandwidth: the disadvantages from ISI outweigh the advantages from energy concentration of double-spike PDP.

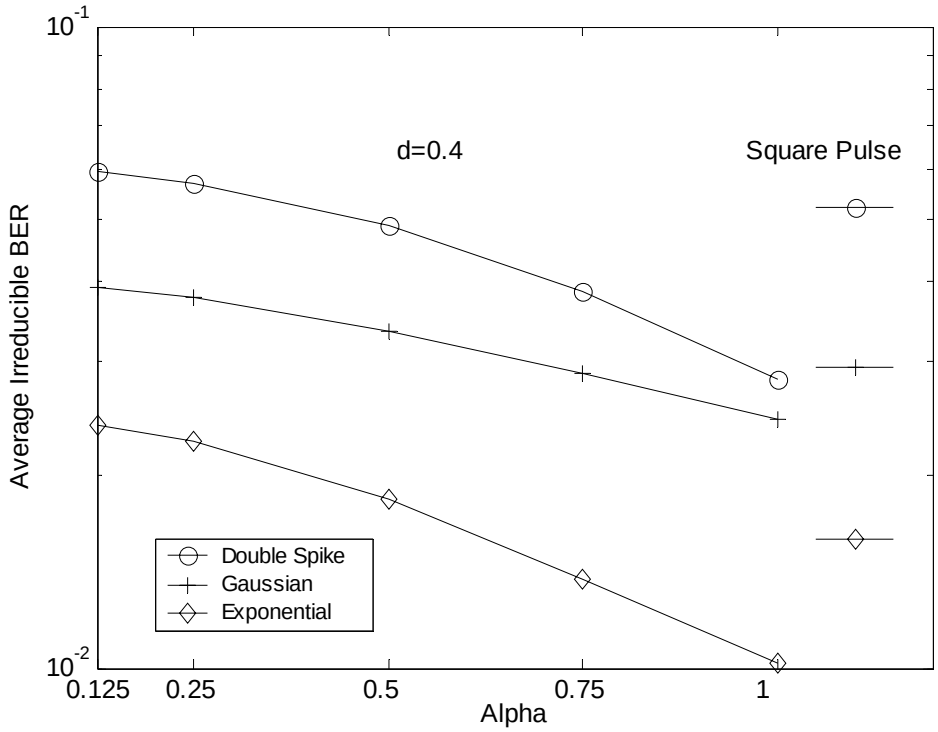

Fig. 6.11 AIBER versus α of RC filter for different PDP and d=0.4.

When *d=0.4*, exponential PDP perform best and double-spike PDP is the worst.

The relative positions of the curves are similar to that in rectangular pulse: double-spike PDP performs best at small RMS delay spread and worst at large RMS delay spread. Overall, AIBER decreases monotonically with the increase of α. The double-spike PDP is most sensitive to α and AIBER will be lowered more obviously with the increase of α. Generally speaking, RC pulse outperform rectangular pulse if $\alpha > 0.75$. A similar conclusion was made in Chuang [31] [32] through simulation.

CHAPTER SEVEN

Conclusions

7.1 Conclusion

In this thesis, the space-time coding scheme presented in [17] is investigated. BER analysis in flat Rayleigh fading channels is summarized. Then AIBER analysis in frequency-selective fading Rayleigh channels is presented. Finally, numerical results prove the accuracy of our analysis and demonstrate STBC can effectively suppress the adverse fading effects.

We assume two transmit antenna and one receive antenna. BPSK modulation is used. QPSK is also considered in the BER analysis for flat Rayleigh fading channels. In frequency-selective Rayleigh fading channels, the suboptimum decoding algorithm in [17] is retained to keep simplicity, which is the advantage of STBC over STTC.

For BER analysis in flat Rayleigh fading channels, some integral results in classic BER analysis for flat fading channels [4] can be applied directly. This analysis result is exact, i.e., no approximation is resorted. One point that should be noted is the definition of SNR per bit. In the thesis, our results are also expressed using the same definition of SNR per bit as [4] in receive diversity using MRC combing. Numerical

results show STBC is only 3 dB inferior to receive diversity using MRC combing when total transmitted power is the same. If the transmitted power on each transmit antenna is the same, then STBC has the same performance as receive diversity using MRC combing.

For frequency-selective Rayleigh fading channels, we presented AIBER analysis of STBC with BPSK modulation. Using our closed form AIBER expression, the effects of various PDP and transmitter/receiver pulse shapes on STBC can be studied in an efficient manner. From our numerical results, we show superior performance of STBC over plain modulation (without space diversity) in frequency-selective Rayleigh fading channels even using a suboptimum decoding algorithm. We also show that the shapes of PDP do not have much effect on AIBER when RMS delay spread is small and RC pulse will outperform rectangular pulse when roll-off factor is greater than 0.75. Overall, STBC is a promising scheme to combat frequency-selective fading.

7.2 Recommendation for Future Works

In this thesis, the sampling time of received signals is locked to τ_{mean} of the PDP. But this may not be the optimum sampling time to achieve minimum AIBER for some PDP. The effect of sampling time on error rate performance can be the subject of future study.

Our AIBER analysis is limited to BPSK modulation, 2 transmit and 1 receive antennas and Rayleigh fading channels. In order to perform AIBER analysis for other modulations, more antennas and other fading channels, more work need to be done.

It is worth to mention that our analyses assume the RMS delay spread is smaller than symbol period. Although this assumption will be valid in many applications, such as short-range radio communications, it weakens the generality of the analysis results when the data rate becomes higher and higher. Error performance analysis for symbol-spaced frequency-selective fading channels can be a new research topic.

The error rate performance analysis of the other category of space-time coding, Space-time Trellis Coding, in frequency-selective fading channels receives little attention. This work is more challenging.

References

[1] T. S. Rappaport, *Wireless Communications Principles and Practice*, 2nd Ed., Prentice-Hall, 2002.

[2] Third Generation Partnership Project, www.3gpp.org.

[3] Third Generation Partnership Project 2, www.3gpp2.org.

[4] J. G. Proakis, *Digital Communications*, 4th Ed., McGraw Hill, 2001.

[5] W. C. Jakes, *Microwave Mobile Communications*, New York: Wiley, 1974.

[6] E. Telatar, "Capacity of multi-antenna Gaussian channels," *European Transactions on Telecommunications,* vol. 10(6), pp. 585-595, Nov/Dec 1999.

[7] G. J. Foschini, Jr. and M. J. Gans, "On limits of wireless communication in a fading environment when using multiple antennas," *Wireless Personal Commun.*, vol. 6, pp. 311–335, 1998.

[8] V. Tarokh, N. Seshadri, A. R. Calderbank, "Space-time codes for high data rate wireless communication: performance criterion and code construction," *IEEE Trans. Inform. Theory*, Vol. 44, pp.744 - 765, Mar 1998.

[9] A.F. Naguib, V. Tarokh, N. Seshadri, A.R. Calderbank, "A space-time coding modem for high-data-rate wireless communications," *IEEE J. Select. Areas Commun.*, Vol. 16, pp. 1459 - 1478, Oct. 1998.

[10] P. S. Henry and B. S. Glance, "A new approach to high capacity digital mobile radio," *Bell Syst. Tech. J.*, vol. 51, pp. 1611–1630, Sept. 1972.

[11] J. H. Winters, “Switched diversity with feedback for DPSK mobile radio systems,” *IEEE Trans. Veh. Technol.*, vol. VT-32, pp. 134–150, Feb. 1983.

[12] A. Wittneben, “Base station modulation diversity for digital SIMULCAST,” in *Proc. IEEE VTC*, pp. 505–511, May 1991.

[13] A. Wittneben, “A new bandwidth efficient transmit antenna modulation diversity scheme for linear digital modulation,” *Proc. IEEE ICC*, pp. 1630–1634, 1993.

[14] Seshadri, N.; Winters, J.H., “Two signaling schemes for improving the error performance of frequency division duplex transmission systems using transmitter antenna diversity,” *IEEE VTC*, May 1993.

[15] J. H. Winters, “Diversity gain of transmit diversity in wireless systems with Rayleigh fading,” *Proc. IEEE ICC*, vol. 2, pp. 1121–1125, 1994.

[16] J.-C. Guey, M. P. Fitz, M. R. Bell, and W.-Y. Kuo, “Signal design for transmitter diversity wireless communication systems over Rayleigh fading channels,” *IEEE Trans. Comm.*, vol. 47, pp. 527-537, Apr. 1999.

[17] S. M. Alamouti, “A simple transmit diversity technique for wireless communications,” *IEEE J. Select. Areas Commun.*, vol. 16, pp. 1451-1458, Oct. 1998.

[18] V. Tarokh, H. Jafarkhani and A. R. Calderbank, “Space-time block codes from orthogonal designs,” *IEEE Trans. Inform. Theory*, vol. 45, pp. 1456-1467, Jul. 1999.

[19] A. Hiroike, F. Adachi, and N. Nakajima, “Combined effects of phase sweeping transmitter diversity and channel coding,” *IEEE Trans. Veh. Technol.*, vol. 41, pp. 170–176, May 1992.

[20] L. J. Cimini, Jr. and N. R. Sollenberger, "OFDM with diversity and coding for high bit-rate mobile data applications," *Proc. 3rd Int. Workshop on Mobile Multimedia Communications*, paper A3.1.1, Sept. 1996.

[21] V. Weerackody, "Diversity for direct-Sequence spread spectrum system using multiple transmit antennas," *Proc. IEEE ICC*, pp. 1775–1779, May 1993.

[22] V. Tarokh, H. Jafarkhani and A. R. Calderbank, "Space-Time Block Coding for Wireless Communications: Performance Results," *IEEE J. Select. Areas Commun.*, vol. 17, pp. 451-460, Mar. 1999.

[23] G. Ganesan, P. Stoica, "Space-Time Block Codes: A Maximum SNR Approach," *IEEE Trans. Inform. Theory*, vol. 47, pp. 1650-1656, May 2001.

[24] H. Shin and J. H. Lee, "Exact Symbol Error Probability of Orthogonal Space-Time Block Codes," *IEEE GLOBECOM*, Taiwan, Dec. 2002.

[25] X. Dong, T. T. Tjhung and F. Adachi, " Error Probability Analysis for 16 STAR-QAM in Frequency-Selective Rician Fading with Diversity Reception," *IEEE Trans. Veh. Technol.*, vol. 47, pp. 924-935, Aug. 1998.

[26] F. Adachi, "BER Analysis of 2PSK, 4PSK, and 16QAM with Decision Feedback Channel Estimation in Frequency-Selective Slow Rayleigh Fading," *IEEE Trans. Veh. Technol.*, vol. 48, pp. 1563-1572, Sept. 1999.

[27] P. A. Bello and B. D. Nelin, "The Effect of Frequency Selective Fading on the Binary Error Probabilities of Incoherent and Differentially coherent Matched Filter Receivers," *IEEE Trans. Comm. Sys.*, vol. 11, pp. 170-186, Jun. 1963.

[28] P. A. Bello and B. D. Nelin, "The Influence of Fading Spectrum on the Binary Error Probabilities of Incoherent and Differentially Coherent Matched Filter Receivers," *IRE Trans. Comm. Sys.*, vol. 10, pp. 160-168, Jun. 1962.

[29] Y. Gong and K. B. Letaief, "Performance evaluation and analysis of space-time coding in unequalized multipath fading links," *IEEE Trans. Comm.*, vol. 48, pp. 1778-1782, Nov. 2000.

[30] P. A. Bello, "Characterization of randomly time variant linear channels," *IEEE Trans. Comm. Sys.*, vol. 11, pp. 360-393, Dec. 1963.

[31] J. C. -I. Chuang, "The effects of time delay spread on portable radio communications channels with digital modulation," *IEEE J. Select. Areas Commun.*, vol. 5, pp. 897-889, Jun. 1987.

[32] J. C. -I. Chuang, "The effects of delay spread on 2-PSK, 4-PSK, 8-PSK and 16-QAM in a portable radio environment," *IEEE Trans. Veh. Technol.*, vol. 38, pp. 1563-1572, Sept. 1989.

[33] Z. Xu, "Space-time block coding over frequency flat and selective Rayleigh fading channels," *M. Eng Thesis of National University of Singapore*, 2002.

[34] A. Vielmon, Y. Li, and J. R. Barry, "Performance of transmit diversity over time-varying Rayleigh-fading channels," *IEEE GLOBECOM*, USA, Dec. 2001.

[35] P. A. Bello and B. D. Nelin, "Binary error probabilities over selectively fading channels containing specular components", *IEEE Trans. Comm. Technol.*, pp. 400-406, Aug. 1966.

Appendix A. Evaluation of Two Complex Integrals

In this appendix, we will prove

$$\int_{-\infty+j\varepsilon}^{\infty+j\varepsilon} \frac{dv}{v+jv_{k1}} = -\pi\, j \tag{A.1}$$

and

$$\int_{-\infty+j\varepsilon}^{\infty+j\varepsilon} \frac{dv}{v-jv_{k2}} = \pi\, j \tag{A.2}$$

We have shown v_{k1} and v_{k2} are real positive numbers. For integrands $\frac{1}{v+jv_{k1}}$ and $\frac{1}{v-jv_{k2}}$, Fig. A.1 identifies the positions of singularities. A circle with radius $R > \max(v_{k1}, v_{k2})$ is drawn on the figure. C_R is the upper half of the circle with radius *R*. Strictly speaking, C_R is slightly less than half circle since the line integral is slightly above the real axis (due to the factor ε). If we use polar coordinate, the radius of C_R is *R* and the angles are in $[\delta, \pi-\delta]$ where δ is a small positive value. We will transform the integral into polar coordinate expression later.

Let's examine $\int_{-R+j\varepsilon}^{R+j\varepsilon} \frac{dv}{v+jv_{k1}}$ and $\int_{-R+j\varepsilon}^{R+j\varepsilon} \frac{dv}{v-jv_{k2}}$. According to residue theorem, the integrals along the semicircle

$$\int_{-R+j\varepsilon}^{R+j\varepsilon} \frac{dv}{v+jv_{k1}} + \int_{C_R} \frac{dv}{v+jv_{k1}} = 0 \tag{A.3}$$

and

$$\int_{-R+j\varepsilon}^{R+j\varepsilon} \frac{dv}{v+jv_{k2}} + \int_{C_R} \frac{dv}{v+jv_{k2}} = 2\pi jRES\left(v_{k2}\right) \tag{A.4}$$

where $RES\left(v_{k2}\right)$ is the residue of $\dfrac{1}{v-jv_{k2}}$ at point jv_{k2}. Apparently, $RES\left(v_{k2}\right)=1$.

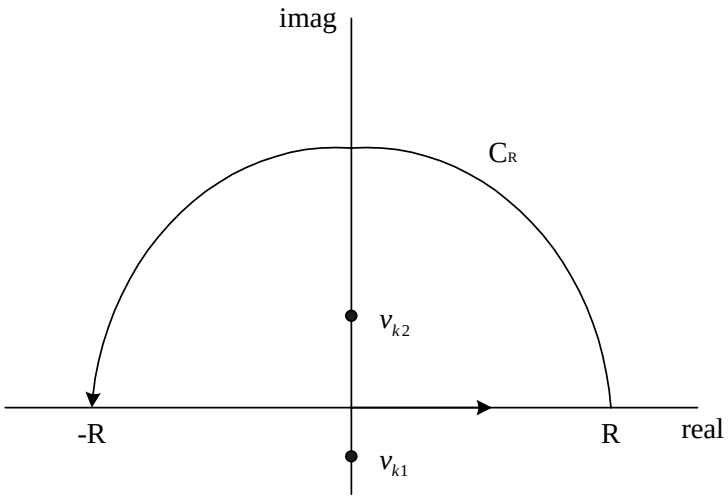

Fig. A.1 Singularities of integrals.

For $\int_{C_R} \dfrac{dv}{v+jv_{k1}}$, we convert Cartesian coordinate into polar coordinate:

$$\int_{C_R} \frac{dv}{v+jv_{k1}} = \int_{\delta}^{\pi-\delta} \frac{\exp(j\theta)\,jRd\theta}{\exp(j\theta)R+jv_{k1}} \tag{A.5}$$

If $R\to\infty$, then $\delta\to 0$,

$$\lim_{R\to\infty}\int_{\delta}^{\pi-\delta} \frac{\exp(j\theta)\,jRd\theta}{\exp(j\theta)R+jv_{k1}} = j\pi \tag{A.6}$$

and (A.3) is directly simplified to (A.1).

Similarly, (A.4) can be simplified to (A.2).

Appendix B. List of Publications

- H.J. Hu, Zhemin Xu and T. T. Tjhung, "Error probability analysis of space time block coding in Frequency Selective Rayleigh Fading Channel," WCNC (IEEE Wireless Communications and Networking Conference), pp. 268-272, New Orleans, USA, March 2003.
- R. Zhang, T. T. Tjhung, H. J. Hu and P. He, "Window function and interpolation algorithm for OFDM frequency offset correction," IEEE Transactions on Vehicular Technology, Vol. 52, pp. 654-670, May 2003. (This work is not included in the thesis.)